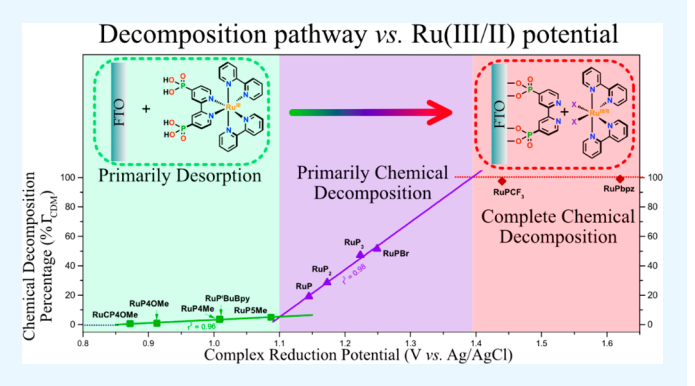


# Fundamental Factors Impacting the Stability of Phosphonate-Derivatized Ruthenium Polypyridyl Sensitizers Adsorbed on Metal **Oxide Surfaces**

McKenzie M. Raber, \*\* Matthew D. Brady, \*\* Ludovic Troian-Gautier, \*\* John C. Dickenson, \*\* Seth L. Marquard, Jacob T. Hyde, Santiago J. Lopez, Gerald J. Meyer, Thomas J. Meyer, Thomas J. Meyer, and Daniel P. Harrison\*,†

Supporting Information

ABSTRACT: A series of 18 ruthenium(II) polypyridyl complexes were synthesized and evaluated under electrochemically oxidative conditions, which generates the Ru(III) oxidation state and mimics the harsh conditions experienced during the kinetically limited regime that can occur in dyesensitized solar cells (DSSCs) and dye-sensitized photoelectrosynthesis cells, to further develop fundamental insights into the factors governing molecular sensitizer surface stability in aqueous 0.1 M HClO<sub>4</sub>. Both desorption and oxidatively induced ligand substitution were observed on planar fluorinedoped tin oxide (FTO) electrodes, with a dependence on the  $E_{1/2}$  Ru(III/II) redox potential dictating the comparative ratios of the processes. Complexes such as RuP4OMe ( $E_{1/2}$  =



0.91 vs Ag/AgCl) displayed virtually only desorption, while complexes such as RuPbpz ( $E_{1/2} > 1.62$  V vs Ag/AgCl) displayed only chemical decomposition. Comparing isomers of 4,4'- and 5,5'-disubstituted-2,2'-bipyridine ancillary ligands, a dramatic increase in the rate of desorption of the Ru(III) complexes was observed for the 5,5'-ligands. Nanoscopic indium-doped tin oxide thin films (nanoITO) were also sensitized and analyzed with cyclic voltammetry, UV-vis absorption spectroscopy, and Xray photoelectron spectroscopy, allowing for further distinction of desorption versus ligand-substitution processes. Desorption loss to bulk solution associated with the planar surface of FTO is essentially non-existent on nanoITO, where both desorption and ligand substitution are shut down with RuP4OMe. These results revealed that minimizing time spent in the oxidized form, incorporating electron-donating groups, maximizing hydrophobicity, and minimizing molecular bulk near the adsorbed ligand are critical to optimizing the performance of ruthenium(II) polypyridyl complexes in dye-sensitized devices.

KEYWORDS: electrochemistry, phosphonate, sensitizer, ruthenium, stability, photoelectrosynthesis, dye-sensitized, interfaces

## INTRODUCTION

Long-lasting and high-efficiency dye-sensitized solar cells (DSSCs) and dye-sensitized photoelectrosynthesis cells (DSPECs) are popular targets in solar fuels production. 1-5 They consist of a multitude of components, both chemical and mechanical, that must work optimally together to become a pragmatic technology. One key component that must be optimized for continued long-term use is the chemical stability of the sensitizer. 6-10 Ruthenium(II) polypyridyl complexes functionalized with phosphonic acids, namely, 4,4'-((HO)<sub>2</sub>(O)- $P)_2-2,2'$ -bipyridine (p-bpy) or  $4,4'-((HO)_2(O)P-CH_2)_2-2,2'$ bipyridine (cp-bpy), 11-14 are used extensively as sensitizers due to their large visible absorbance, well-understood photophysical properties, and reversible one-electron transfer chemistry. 15–18

In DSSCs and DSPECs, oxidative equivalents are generated after excited-state electron injection from the adsorbed

sensitizer RuIIL to the metal oxide nanocrystallite acceptor states (Figure 1A). 19,20 The oxidized sensitizer Ru<sup>III</sup>L is then reduced by an external redox mediator (as in DSSCs) or reductant (as in DSPECs) to regenerate RuIIL. 21,22 The process can then be repeated to produce current and the corresponding solar fuels. In either application, Ru<sup>III</sup>L is a short-lived transient species with a finite lifetime under steady-state conditions. In many cases, the long-term performance of sensitizer-catalystbased DSPEC for water oxidation is limited by the stability of the oxidized sensitizer. 23,24 An understanding of the origin, rates, mechanisms, and products of these deleterious decomposition pathways is important to increase device longevity.

Received: March 20, 2018 Accepted: June 8, 2018 Published: June 8, 2018



<sup>&</sup>lt;sup>†</sup>Department of Chemistry, Virginia Military Institute, Lexington, Virginia 24450, United States

Department of Chemistry, University of North Carolina at Chapel Hill, Chapel Hill, North Carolina 27599, United States

**ACS Applied Materials & Interfaces** 

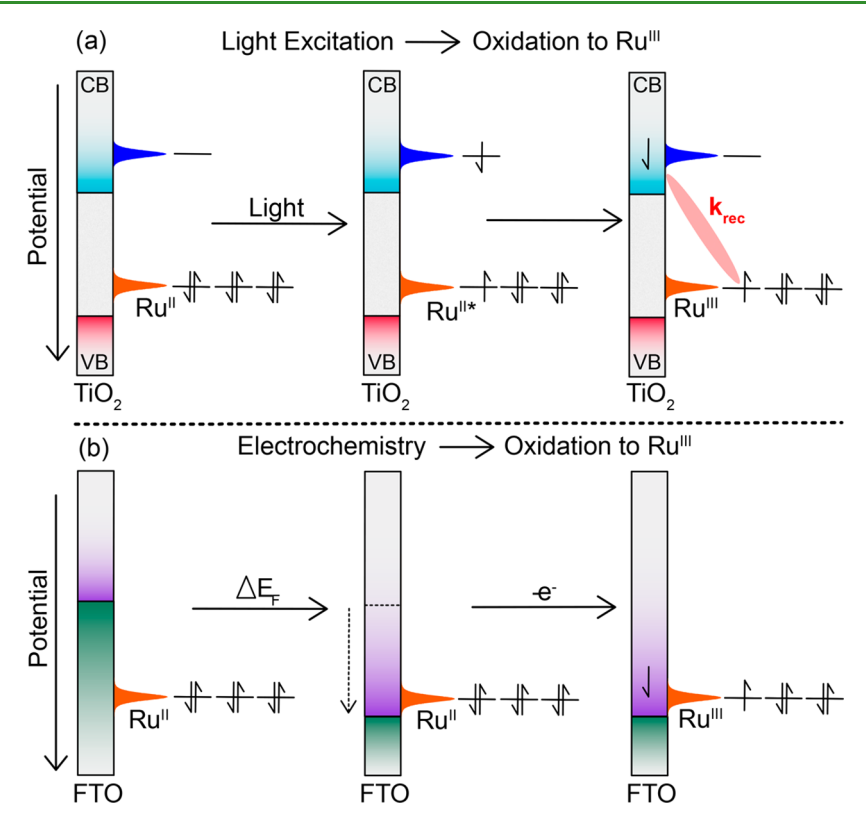
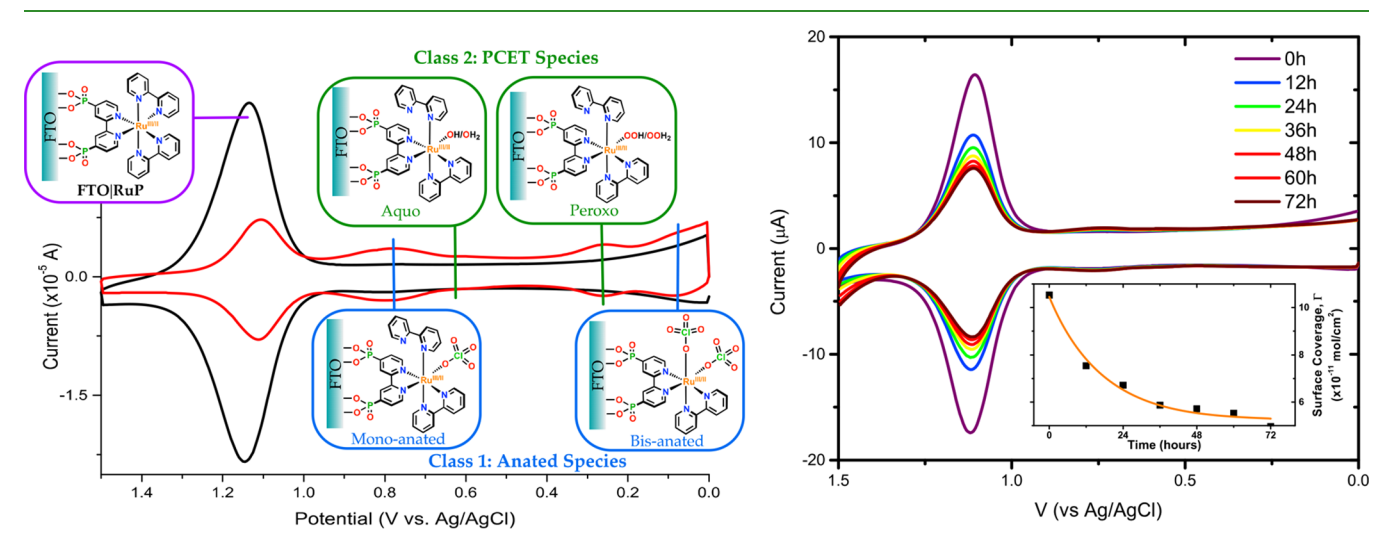


Figure 1. Comparison of transient formation of  $Ru^{III}$  by (A) photoexcitation of a  $Ru^{II}$  sensitizer on  $TiO_2$  to  $Ru^{II*}$  and excited-state electron injection (CB is conduction band, VB is valence band, and  $k_{\rm rec}$  represents the recombination rate constant associated with back electron-transfer processes) and (B) electrochemical oxidation on FTO. The teal shading indicates the Fermi potential of the electrode, and the orange distribution curves indicate the density of states for  $Ru^{II}$ .



**Figure 2.** CV overlays of FTOl**RuP** prior to (black) and following (red) 12 h of a 1.5 V (vs Ag/AgCl) applied potential electrochemical protocol described in experimental details (left). Classes of electrochemically active chemical decomposition products are indicated along with their corresponding redox potentials. Class 1 FTOl**RuP-CDPs** in blue are monoanated and bis-anated species at  $E_{1/2} = 0.8$  and 0.05 V, respectively, while aquo- and peroxo-PCET, CDPs are highlighted in green with  $E_{1/2} = 0.65$  and 0.25 V, respectively. CV overlays of FTOl**RuP** collected every 12 h for 3 d, without an applied potential, indicating Ru(II) chemical stability (right). (inset) The surface coverage as a function of time.

These parameters can be studied using electrochemistry, where  $\mathbf{Ru^{II}}\mathbf{L}$  is oxidized to  $\mathbf{Ru^{III}}\mathbf{L}$  (Figure 1B) using a conductive fluorine-doped tin oxide (FTO) electrode. Electrochemistry on FTO is a very convenient method to approximate harsh conditions, where DSSCs and DSPECs are not efficiently supplied with reducing agents fast enough to regenerate  $\mathbf{Ru^{II}}\mathbf{L}$ , and effectively allows one to model the long-term behavior of  $\mathbf{Ru^{III}}\mathbf{L}$ .

We previously reported on the electrochemical stability of a handful of ruthenium-based sensitizers adsorbed on FTO, focusing primarily on the factors effecting the stability of FTOl  $[Ru^{II}(4,4'-((HO)_2(O)P)_2bpy)(bpy)_2]^{2+}$  (FTOlRuP).<sup>23</sup> Desorption was the only loss mechanism for FTOlRuP in the Ru(II) oxidation state while oxidatively induced ligand substitution and/or desorption were responsible for accelerated losses upon oxidation to Ru(III). Pourbaix analysis of redox

**ACS Applied Materials & Interfaces** 

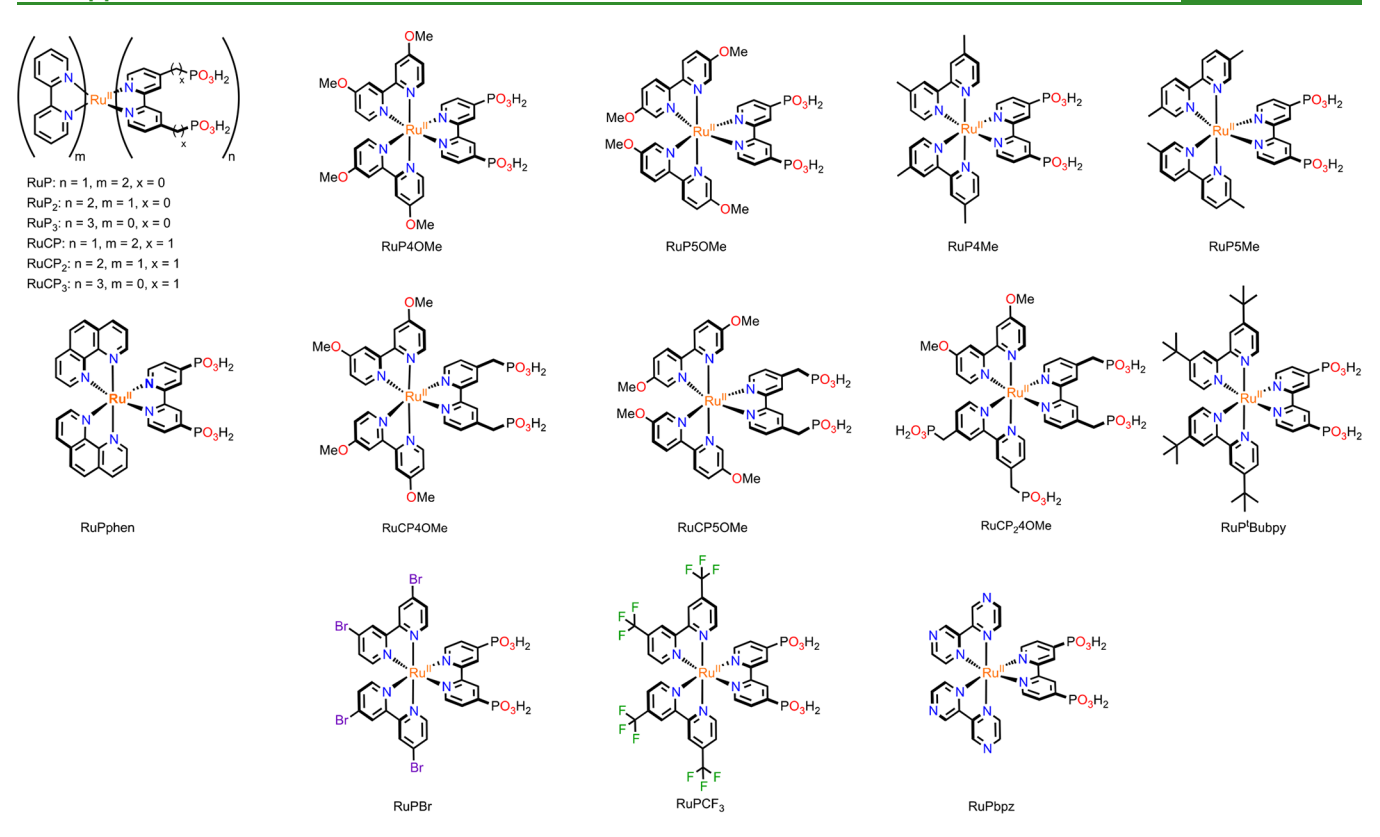


Figure 3. Ruthenium sensitizers used in this study that all possess either a 4,4'-((HO)<sub>2</sub>(O)P)<sub>2</sub>-2,2'-bipyridine or a 4,4'-((HO)<sub>2</sub>(O)P-CH<sub>2</sub>)<sub>2</sub>-2,2'bipyridine to allow for surface anchoring. Substitutions of the ancillary ligands allow for the tunability of their redox potential, hydrophobicity/ hydrophilicity, and steric arrangements.

couples generated upon oxidation revealed two general classes of electrochemically active chemical decomposition products (CDPs), FTO|RuP-CDPs, resulting from ligand substitution: anated species (where electrolytic perchlorate entered the coordination sphere; Class 1) and proton-coupled electron transfer (PCET) complexes (consisting of aquo- and peroxo-Ru coordinated ligands; Class 2) (Figure 2).

In this study, a series of 18 ruthenium sensitizers (Figure 3) bearing phosphonic acid anchoring groups were used to investigate the steric and electronic factors at stake for preventing sensitizer desorption as well as decomposition in pH 1 aqueous perchloric acid solutions (0.1 M HClO<sub>4</sub>). Substitutions at the 4,4'- or 5,5'-positions on the 2,2'-bipyridine ancillary ligands allowed tuning of both the redox potential as well as the bulkiness and hydrophobicity/hydrophilicity of the corresponding ruthenium sensitizer. Additionally, our attempts to deconvolute the various decomposition processes responsible for the oxidatively induced loss of FTO|RuL are described below.

# RESULTS

# Equations Governing the Decomposition Processes.

Rate constants  $k_d$  for the loss of several sensitizers, namely, FTOI  $RuP_{1\rightarrow 3}$  and  $FTO|RuCP_{1\rightarrow 3}$ , were previously determined using a 12 h electrochemical protocol monitoring the surface coverage as a function of time spent in the Ru(III) state (eq 1).23 The same electrochemical data monitored the formation of FTOI RuL-CDPs (CDP is chemical decomposition products) and indicated a buildup of FTO|RuL-CDPs over the course of the experiment (eq 2a; see Figure S1). A surface coverage difference  $(\Delta\Gamma)$  between the consumption of FTO**RuP** and the formation

of FTOlRuL-CDPs indicated that electrochemically silent processes were concomitantly occurring. Likely processes included (i) direct desorption of the intact RuL fragment (eq 2b) or (ii) complete ligand substitution at the adsorbed ligand coordination sites (eq 2c). Hence,  $k_d$  encompasses  $k_{2a}$ ,  $k_{2b}$ , and  $k_{2c}$  but is impossible to deconvolute electrochemically. The electron-transfer rate constants  $k_{1,ET}$  were determined by Laviron analysis (see Table S1 and Figures S2-S16). 25,26

$$FTO|RuL^{2+} \xrightarrow{k_{1,ET}} FTO|RuL^{3+} + e^{-}$$
 (1)

$$FTO|RuL^{3+} \xrightarrow{k_{2a}} FTO|RuL-CDPs \text{ (class1 and 2 CDPs)}$$
 (2a)

$$FTO|RuL^{3+} \xrightarrow{k_{2b}} FTO| + RuL^{3+}$$
 (desorption, e-chem silent) (2b)

$${\rm FTOlRuL^{3+}} \xrightarrow{k_{2c}} {\rm FTOlp\text{-}bpy} + {\rm RuL\text{-}CDPs}$$

Eventually, the formation of the FTOIRuL-CDPs stalls as the amount of FTO|RuL decreases, at which point, they too begin converting to electrochemically silent species via desorption (eq 3a) or to FTOlp-bpy (eq 3b; see Figure S1). It is noteworthy that the FTO|RuL-CDPs are interconverting.

$$FTO|RuL-CDPs \rightarrow FTO| + RuL-CDPs$$
(slow; desorption, e-chem silent) (3a)

$$FTO|RuL-CDPs \rightarrow FTO|p-bpy + RuL-CDPs$$

(slow; adsorbed ligand substitution, e-chem silent)

(3b)

FTO|RuL-CDPs 
$$\rightarrow$$
 FTO|RuL-CDPs-2 (slow; CDP interconversion) (3c)

Because the processes in eq 3 are much slower than those of eq 2, the maximum percentage of conversion of FTO|RuL  $\rightarrow$ FTOlRuL-CDPs can be utilized as a means to compare the stability of the sensitizers according to eq 4.

$$\%\Gamma_{\rm cdm} = \frac{\sum (\Gamma_{\rm all\ decomp})}{\Gamma_{{\rm chr},t=0}} \times 100 \tag{4}$$

In eq 4,  $%\Gamma_{cdm}$  represents the maximum surface coverage of electrochemically active FTO|RuL-CDPs over the time scale of a given experiment,  $\sum (\Gamma_{\text{all decomp}}) = \Gamma(\text{FTO}|\text{RuL}-\text{OH}_2) +$  $\Gamma(FTO|RuL-OOH) + \Gamma(FTO|RuL-OCIO_3) + \Gamma(FTO|RuL-OCIO_3)$  $(OClO_3)_2$ ), and  $\Gamma_{chr,t=0}$  represents the initial surface coverage of the sensitizer.

While  $%\Gamma_{cdm}$  quantifies electrochemically active decomposition products, monitoring the overall retention of FTO|RuL according to eq 5 captures both electrochemically active and inactive processes. Hence, the surface coverage retention percentage,  $%\Gamma_{ret}$  provides another useful metric for analyzing and comparing sensitizers.

$$\%\Gamma_{\rm ret} = \frac{\Gamma_{\rm chr}}{\Gamma_{{\rm chr},t=0}} \times 100 \tag{5}$$

Perfectly electrochemically stable sensitizers, and by extension excellent DSSC/DSPEC targets, would have a  $\%\Gamma_{\rm ret} = 100$ , a corresponding  $%\Gamma_{\rm cdm} = 0$ , and a  $k_{\rm d} = 0~{\rm s}^{-1}$ . Using these three metrics,  $\%\Gamma_{\rm ret}$   $\%\Gamma_{\rm cdm}$ , and  $k_{\rm d}$ , we are able to quantifiably describe key FTOlRuL steric and electronic factors effecting a sensitizer's electrochemical stability on FTO.

**Electronic Effects.** Redox Potential Impact. A strong linear correlation between  $k_d$  and the sensitizer's Ru(III/II) redox potential as well as a strong linear correlation between the  $\Gamma_{\rm cdm}$  and  $E_{1/2}$  (Figure 3) for the series FTOlRuP<sub>1→3</sub> was observed. No correlation was observed between  $%\Gamma_{\text{ret}}$  and the Ru(III/II) redox potential. Nonetheless, raising the Ru(III/II) redox potential with electron-withdrawing groups increased the rates and total amounts of decomposition of the Ru(III) state.

Extrapolation of the linear fitting (Figure 4) indicated that  $k_d$ and  $\%\Gamma_{cdm}$  reach values of 0 when the RuL(III/II) redox

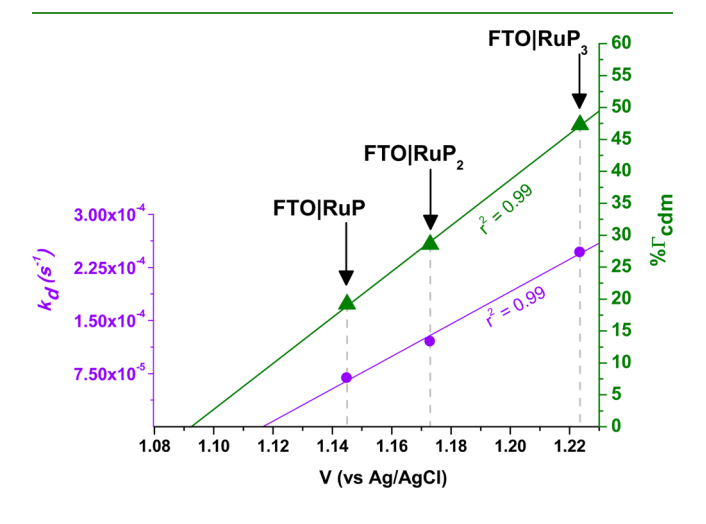


Figure 4. Correlation between (1)  $k_d$  and FTO|RuP<sub>1 $\rightarrow$ 3</sub> Ru(III/II) redox potential (ullet) and (2) % $\Gamma_{cdm}$  as a function of FTO| $RuP_{1\rightarrow 3}$ Ru(III/II) redox potential ( $\blacktriangle$ ).

potentials reach 1.12 and 1.09 V versus Ag/AgCl, respectively. Complete conversion to FTO|RuL-CDPs (i.e.,  $\%\Gamma_{cdm} = 100$ ) was estimated to occur when a RuL(III/II)  $E_{1/2} = 1.37$  V versus Ag/AgCl, which corresponds to a rapid  $k_d = 5.8 \times 10^{-4} \text{ s}^{-1}$ .

To verify these extrapolations, a series of Ru-based sensitizers bearing 4,4'-substituted-2,2'-bipyridine ligand was subjected to a 12 h electrochemical protocol (see experimental details). The reduction potential of this series of ruthenium sensitizers ranged from 0.87 to more than 1.62 V versus Ag/AgCl. Results concerning the electrochemical stability of these ruthenium sensitizers are found in Table 1.

As can be observed from Table 1, a very limited amount of chemical decomposition occurred by using sensitizers with Ru(III/II) reduction potentials below the 1.12/1.09 threshold (e.g., FTOlRuP4Me, FTOlRuP4OMe, FTOlRuCP4OMe, and FTOlRuP4<sup>t</sup>Bubpy). Interestingly, plotting the limited chemical decomposition percentage (% $\Gamma_{cdm}$ ) of these sensitizers as a function of  $E_{1/2}$  (Figure 5) gave rise to a trend that was independent of  $FTO|RuP_{1\rightarrow 3}$ . The observed trend intersected with the FTO $|RuP_{1\rightarrow 3}|$  series at 1.10 V (Figure 5). It is important to note that no significant differences in  $k_d$  were observed within the FTO|Ru4L series, that is, where 4,4'-substituted-2,2'bipyridine ancillary ligands with electron donating groups are used.

FTOlRuPCF<sub>3</sub> ( $E_{1/2} = 1.44 \text{ V}$ ) and FTOlRuPbpz ( $E_{1/2} > 1.62$ V), with Ru(III/II) redox potentials above the projected 1.37 V threshold, led to complete decomposition to FTOlRuL-CDPs 2–3 orders of magnitude faster than all other sensitizers. While chemical decomposition was measurable with FTOlRuPCF<sub>3</sub> chemical decomposition was extremely rapid (i.e., seconds) with FTO|RuPbpz as conversion to FTO|RuPbpz-CDPs only required scanning through the FTOlRuIII/IIPbpz couple. Note that no FTOlRuIII/IIPbpz redox potential was observed due to the rapid electrochemical decomposition. Using a comparably sized sensitizer, RuP, as an estimate of the maximum surface coverage  $\Gamma_{\text{max}}$  we estimated  ${\sim}99\%\Gamma_{\text{cdm}}$  for FTOlRuPbpz (RuP,  $\Gamma_{\text{max}} = 1.12 \times 10^{-10} \text{ mol/cm}^2$ ; RuPbpz-CDPs,  $\Gamma_{\text{cdm}} = 1.11 \times$  $10^{-10}$  mol/cm<sup>2</sup>). FTOl**RuPBr** ( $E_{1/2} = 1.25$  V) fits well with the FTO| $RuP_{1\rightarrow 3}$  series.

**Structural Effects.** The overall stability and the rates of decomposition of the ruthenium sensitizers under applied potential were investigated with regard to parameters such as steric effects, hydrophobicity/hydrophilicity, as well as the rigidity of the different ligands

**Functional Group Effects.** The influence of steric bulk was investigated using a series of ruthenium sensitizers bearing 5,5'substituted-2,2'-bipyridine. Remarkably, FTOlRuP5OMe and FTO|RuCP5OMe were both lost within 30 min of an applied potential hold. Thus, applied potential holds for a duration of only 4 min in 1 min intervals were used to yield similar  $%\Gamma_{ret}$  to the 12 h electrochemical protocol analogues. Loss of both FTO RuP5OMe and FTO|RuCP5OMe occurred ~100 times faster than their 4,4'-analogues, FTO|RuP4OMe and FTO|RuC-P4OMe, upon oxidation to Ru(III), while loss of FTO|RuP5Me was nearly identical to FTOlRuP4Me (Table 2). FTOl RuP5Me, FTOlRuP5OMe, and FTOlRuCP5OMe all exhibit reduction potentials close to FTO|RuP and thus should decompose on a similar time scale. Therefore, Ru(III) stability is extremely sensitive to functional group such that just a subtle change in bulk from a methyl to a methoxy group at the 5,5'positions increases the decomposition rate by 100-1000. As expected, the functional group identity of the 4,4'-positions is sterically inconsequential.

Table 1. Redox Potentials Measured in Aqueous 0.1 M HClO<sub>4</sub> for a Series of Ruthenium Sensitizers Adsorbed on FTO Electrodes<sup>a</sup>

FTOlRuL	$E_{1/2}(\mathrm{Ru^{III/II}}\mathrm{L})~[\Delta E_{1/2}]~(\mathrm{V}~\mathrm{vs}~\mathrm{Ag/AgCl})$	$k_{\rm d} \left[ \frac{k_{\rm d}(\rm FTO RuL)}{k_{\rm d}(\rm FTO RuP)} \right]$	$\%\Gamma_{ m ret,app}$	$\%\Gamma_{ m ret,ctrl}$	$\%\Gamma_{ m cdm}$
FTOlRuCP4OMe	0.872 [-0.274]	$5.5 \times 10^{-5} [7.9]$	20	83	1
FTOlRuCP <sub>2</sub> 4OMe	0.903 [-0.243]	$3.6 \times 10^{-5} [5.2]$	21	82	Ь
FTOlRuP4OMe	0.913 [-0.232]	$5.7 \times 10^{-5} [8.3]$	27	84	1
FTO RuP <sup>t</sup> Bubpy	1.008 [-0.138]	$5.2 \times 10^{-5} [7.5]$	33	99	3
FTOlRuP4Me	1.009 [-0.137]	$6.2 \times 10^{-5} [9.0]$	34	82	4
FTOlRuPBr	1.249 [+0.104]	$1.2 \times 10^{-4} [17]$	6	92	52
FTO RuPCF <sub>3</sub>	1.440 [+0.295]	$9.6 \times 10^{-3} [1400]^c$	16	90	81 (98 <sup>d</sup> )
FTOlRuPbpz	>1.62 [>+0.475]	$N/A^e$	<1	unknown <sup>f</sup>	99

<sup>a</sup>Their difference relative to FTO|RuP is found in brackets ( $\Delta E_{1/2} = E_{1/2}(\text{FTO}|\text{RuL}) - E_{1/2}(\text{FTO}|\text{RuP})$ ), their associated rate constant  $k_{\rm d}$  and rate constant ratio relative to FTO|RuP are located in brackets, the surface coverage percentages (%Γ<sub>ret,app</sub>) after an applied potential electrochemical protocol (see experimental details), the surface coverage percentage (%Γ<sub>ret,ctrl</sub>) of an electrode without an applied potential hold, and maximum surface coverage percentage of electrochemically active FTO|RuL-CDPs (%Γ<sub>ret,ctrl</sub>) of corresponding electrodes are presented. Unless otherwise noted, these values represent 12 h experiment times. <sup>b</sup>Like FTO|RuCP<sub>1→3</sub>, ligand oxidation complicates quantification of decomposition products (see broadening in Figure S17). <sup>c</sup>Experiment time of 4 min. <sup>d</sup>Calculated %Γ<sub>cdm</sub> considering 84% of the FTO|RuPCF<sub>3</sub> reacted (100%–16%Γ<sub>ret</sub>). <sup>e</sup>Experiment time of seconds. <sup>f</sup>The value is unmeasurable due to rapid decomposition accompanying scanning through the anodic wave.

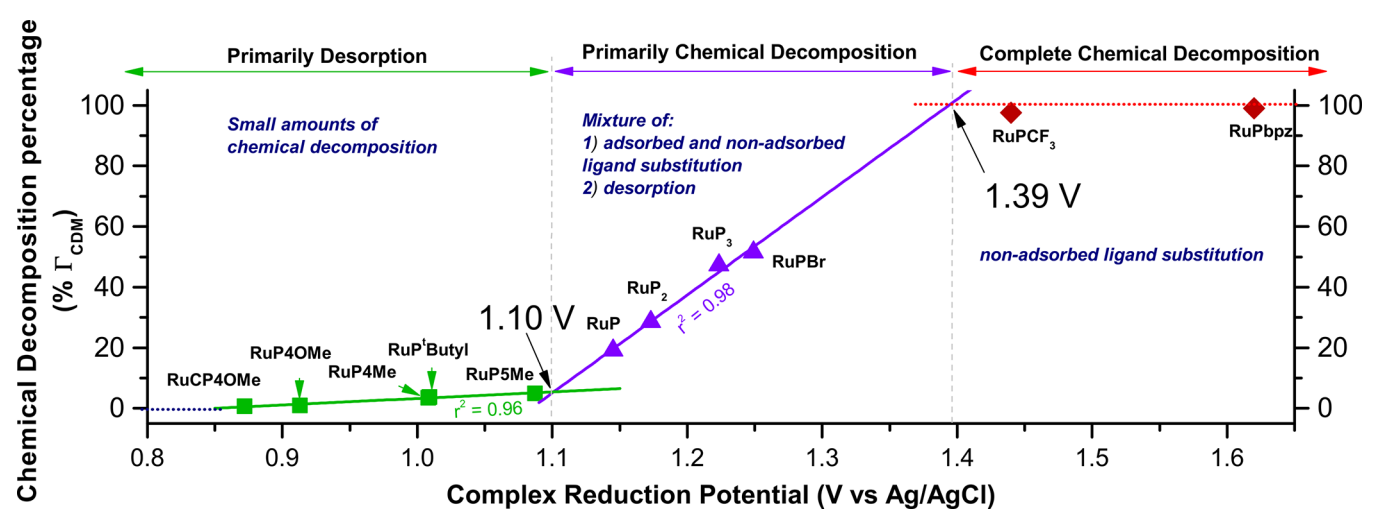


**Figure 5.** Correlation between the observed chemical decomposition percentage and the reduction potential of a series of ruthenium sensitizers bearing 4,4′-substituted-2,2′-bipyridine on FTO. Experiments were performed in aqueous 0.1 M HClO<sub>4</sub> following a 12 h electrochemical protocol. The experiment time for FTOlRuPCF<sub>3</sub> was 4 min and was several seconds for FTOlRuPbpz.

Table 2. Redox Potentials Measured in Aqueous 0.1 M HClO<sub>4</sub> for a Series of Rapidly Decomposing Ruthenium Sensitizers Adsorbed on FTO Electrodes<sup>a</sup>

FTOlRuL	$E_{1/2}(\mathrm{Ru^{III/II}}L)~[\Delta E_{1/2}]~(\mathrm{V}~\mathrm{vs}~\mathrm{Ag/AgCl})$	$k_{\rm d} \left[ \frac{k_{\rm d}({\rm FTO RuL})}{k_{\rm d}({\rm FTO RuP})} \right]$	$\%\Gamma_{ ext{ret,app}}$	$\%\Gamma_{ m ret,ctrl}$	$\%\Gamma_{ m cdm}$
FTO RuCP5OMe	1.051 [-0.094]	$7.7 \times 10^{-3} [1100]$	23	90	43
FTOlRuP5Me <sup>b</sup>	1.087 [-0.059]	$6.9 \times 10^{-5} [10]$	26	66	5
FTOlRuP5OMe	1.123 [-0.023]	$7.9 \times 10^{-3} [1200]$	21	94	22
FTOlRuPphen	1.135 [-0.011]	$5.3 \times 10^{-3} [770]$	27	86	64

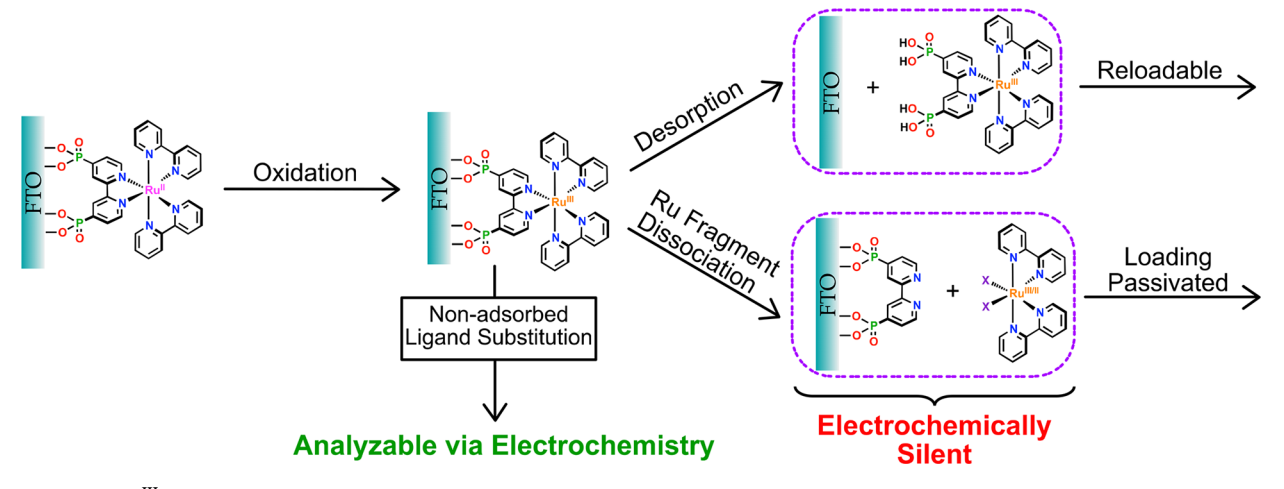
<sup>&</sup>lt;sup>a</sup>Rate constant and surface coverages of the corresponding electrodes following a 4 × 1 min electrochemical protocol (see experimental details), unless otherwise noted. <sup>b</sup>Experiment time of 12 h.

**Hydrophobic Effect.** Of the initial survey, FTOlRuP4Me was the only sensitizer that retained significantly more material than FTOlRuP and other analogous compounds in a 12 h period (% $\Gamma_{\text{ret}} = 34 \text{ vs } 20\%\Gamma_{\text{ret}}$  on average). Suspecting a hydrophobic effect for the enhanced retention, FTOlRuP<sup>t</sup>Bubpy was investigated, as the 4,4'-di-*tert*-butyl groups would increase the hydrophobicity of the RuP fragment significantly. The  $k_d$  was found to be very similar to other FTOlRuLs systems (Table 1)

with limited chemical decomposition ( $5\%\Gamma_{cdm}$ ), consistent with its reduction potential (1.008 V). Retention of FTOl  $\mathbf{Ru^{III}P^tBubpy}$  ( $33\%\Gamma_{ret}$ ) was not better than FTOl $\mathbf{Ru^{III}P^tMe}$  ( $34\%\Gamma_{ret}$ ), but a more significant effect was observed for the retention of the FTOl $\mathbf{Ru^{II}P^tBubpy}$  ( $99\%\Gamma_{ret}$  vs  $82\%\Gamma_{ret}$  (FTOl  $\mathbf{Ru^{II}P^tMe}$ )).

**Ligand Rigidity.** Class 1 and Class 2 decomposition products are formed via partial or complete ligand substitution

Scheme 1. Oxidatively Induced Decomposition Pathways Leading to Loss of the Electrochemically Active Redox Couples from the FTO Electrode



"Desorption of RuIIL leads to a surface that can be reloaded with new RuLs, while dissociation of the ruthenium fragment blocks loading sites on the electrode surface. Note that decomposition products that are analyzable via electrochemistry are represented in Figure 2 (left).

of the non-adsorbed ancillary ligands. With 2,2'-bipyridine derivatives, this decomposition must necessarily undergo a  $\kappa^2 \to$  $\kappa^1$  isomerization to generate Class 1 decomposition products, while complete ligand loss, presumably via  $Ru^{II}(\kappa^2-p-bpy)(\kappa^2-p-bpy)$ bpy)( $\kappa^1$ -bpy)(X), results in Class 2 decomposition products. We anticipated that geometrically restricting the C-C rotation using 1,10-phenanthroline (phen) would greatly enhance the stability of complexes by preventing one decomposition mechanism (Figure S18). To the contrary, decomposition of FTO|RuPphen is nearly three orders of magnitude faster than its 2,2'-bipyridine analogue (FTO|RuPphen:  $k_d = 5.3 \times 10^{-3}$  $s^{-1}$ ; FTO|RuP:  $k_d = 6.9 \times 10^{-6} s^{-1}$ ; Table 2). The reduction potentials of FTO|RuP and FTO|RuPphen are nearly identical, yet there is a dramatically different rate of decomposition.

Distinguishing Loss Mechanisms. In all cases,  $%\Gamma_{\rm ret}$  +  $\%\Gamma_{\rm cdm} \neq 100$  when the complexes  $E_{1/2}$  is less than 1.39 V. At least two electrochemically silent conversions (e.g., eqs 2b and 2c) are responsible for the difference and are indistinguishable electrochemically (Scheme 1). These proposed processes are distinct in that one completely desorbs the sensitizer from the surface (eq 2b), opening adsorption sites, while the second leads to p-bpy still present at the surface (eq 2c). In an unsophisticated approach, reloading the electrodes with an electrochemically active complex should indicate the extent to which free adsorption sites were made available during the oxidation process (Scheme 1).

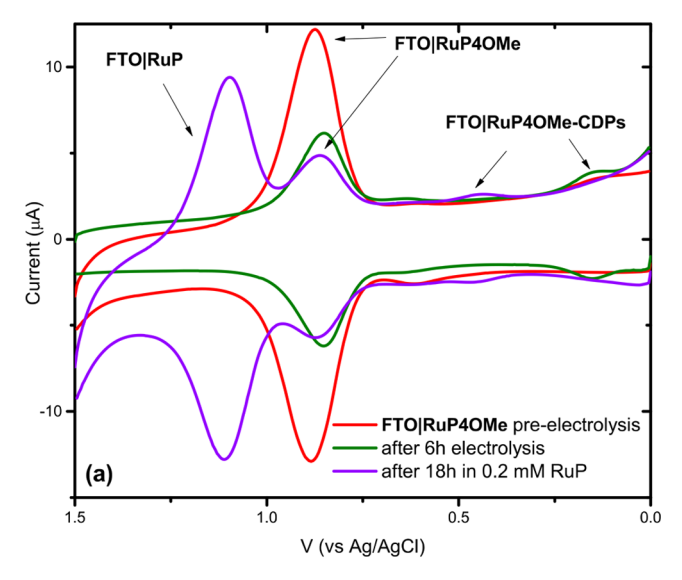
Therefore, several FTOlRuLs were subjected to an applied potential for a time sufficient to decompose the majority of the sensitizer, and these electrodes were then placed into a loading solution of RuP for 18 h. Figure 6 shows the cyclic voltammograms (CVs) for two extreme examples, namely, FTO|RuP4OMe and FTO|RuP3. FTO|RuP4OMe exhibited a significant uptake of RuP ( $\sim 50\%\Gamma_{max}$ ), and  $\sim 90\%$  surface coverage was recovered  $(49\%\Gamma_{max}(RuP) +$  $40\%\Gamma_{\rm ret}({\bf RuP4OMe}))$ . At the other extreme, only 24%  $(12\%\Gamma_{\text{max}}(\text{RuP}) + 12\%\Gamma_{\text{ret}}(\text{RuP}_3))$  of surface coverage was recovered when a similar procedure was used on FTO|RuP<sub>3</sub>. An FTO|RuP electrode oxidized for 6 h (33% $\Gamma_{ret}$ ) reloaded to  $79\%\Gamma_{max}$ , whereas FTO|RuP<sub>2</sub> oxidized for 2.5 h  $(33\%\Gamma_{\text{ret}}(\text{RuP}_2))$  reloaded to  $59\%\Gamma_{\text{max}}$   $(40\%\Gamma_{\text{max}}(\text{RuP})$  + 19%Γ<sub>ret</sub>(RuP<sub>2</sub>)). FTOlRuPCF<sub>3</sub>, FTOlRuPbpz, and FTOl

RuP5OMe also reloaded to  $25-30\%\Gamma_{max}\left(RuL+RuP\right)$  when soaked in RuP for 18 h.

From these data, complete or nearly complete ligand-based chemical decomposition (FTO|RuL → FTO|RuL-CDPs + FTOlp-bpy) occurred in complexes with high  $E_{1/2}$  approaching or exceeding 1.39 V (FTOlRuP3, FTOlRuPCF3, FTOl RuPbpz), and sterically driven loss (FTO|RuP5OMe), while the primary loss mechanism is desorption (FTOIRuL  $\rightarrow$  FTOI + **RuL**) in complexes with  $E_{1/2}$  < 1.10 V.

To gain further evidence for the two mechanisms at stake for the ligand-based chemical decomposition, we decided to replace the bare FTO electrode with a nanoscopic indium doped tin oxide thin film (nanoITO) electrode. The surface area of nanoITO allowed an increase in the surface coverage and changes in the visible absorption to be monitored before, upon, and after oxidation. Furthermore, X-ray photoelectron spectroscopy (XPS) analysis on nanoITO surfaces sensitized with ruthenium complexes allowed for better signal/noise ratios than when FTO was used. XPS as well as changes in the metal-toligand charge transfer (MLCT) maximum are gathered in Table 3 (see Figures S19-S24).

The nitrogen and phosphorus ratios obtained by XPS before oxidation were all in agreement with the expected ratio based on the molecular structure. After 12 h of oxidation, this ratio was affected to different magnitudes. For nanoITOlRuP4OMe, a very slight increase was observed, while the absorbance at the MLCT maximum before and after oxidation remained unchanged. Changing the substituents from the 4,4'-position to the 5,5'-position, that is, nanoITO|RuP5OMe resulted in significantly different results. Indeed, the nitrogen and phosphorus ratio remained almost unchanged, but the absorption drastically decreased to reach 40% of its initial value, that is, from 1.39 pre-oxidation to 0.56 post-oxidation. A similar observation was made for nanoITOlRuP, where 50% of the initial absorption value remained after 12 h of oxidation. In the case of nanoITO|RuP<sub>3</sub> and nanoITO|RuPbpz, both surfaces exhibited a decrease in their MLCT absorption accompanied by a drastic increase in their nitrogen and phosphorus ratio relative to ruthenium.



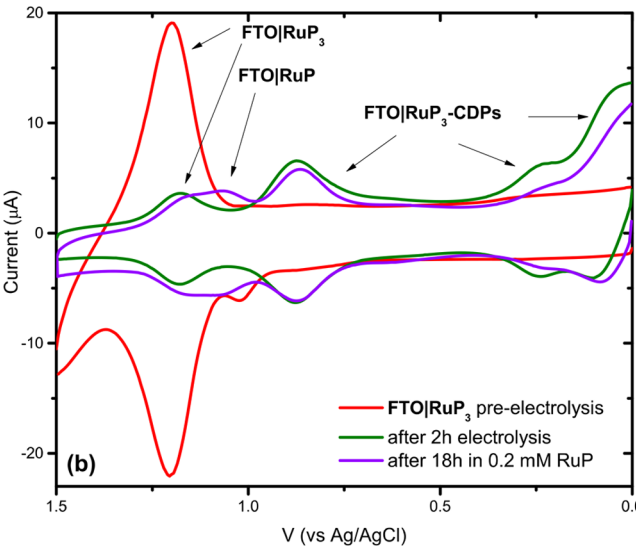


Figure 6. CVs of FTOlRuP4OMe (a) and FTOlRuP3 (b) before (red) the applied potential and after (green) bulk electrolysis experiments  $(t_{app} = 6 \text{ and } 2 \text{ h, respectively})$  leading to desorption and decomposition. Surfaces are then soaked for 18 h in a solution of RuP, and CVs (purple) are recorded again to estimate the new surface coverages and the amount of compound loss during bulk electrolysis.

## **DISCUSSION**

The electrochemical stability of 18 ruthenium(II) sensitizers was investigated to assess the factors that influence the decomposition of the sensitizers in DSSCs or DSPECs devices. The study was performed under conditions that should simulate the harsh conditions where oxidized sensitizers are not rapidly regenerated to their original oxidation state. Factors that were investigated include the redox potential of these sensitizers as well as structural factors such as ligand rigidity, bulkiness, and hydrophobicity/hydrophilicity. Surface coverage dependency, as well as XPS and spectro-electrochemistry, further allowed to tease out, at least partially, the different pathways involved in the decomposition mechanisms.

Electrochemical Effects. Data gathered in Figure 5 allowed for the extrapolation of three different regimes that were operative at potentials centered around 1.10 and 1.39 V (vs Ag/ AgCl). Sensitizers that possessed a redox potential greater than 1.39 V versus Ag/AgCl degraded 2-3 orders of magnitude faster

Table 3. Atomic Distribution (Normalized to Ruthenium) of Ru, N, and P for Indicated Systems on nanoITO before and after a 12 h, unless Otherwise Noted, Applied Potential,  $E_{app}$ , Hold Past Their  $E_{1/2}^{\phantom{1}a}$ 

system	$E_{1/2}$ (V vs Ag/AgCl)	Ru	N	P	abs at MLCT
RuP4OMe	0.913	1	6.8 (6)	2.0(2)	0.72
RuP4OMe (post $E_{app}$ hold)		1	8.3	2.8	0.72
RuP5OMe	1.125	1	6.1 (6)	1.9(2)	1.39
RuP5OMe (post $E_{app}$ hold)		1	8.0	2.8	0.56
RuP5OMe + p-bpy <sup>b</sup>		1	14.7	8.3	0.26
RuP	1.145	1	6.0 (6)	1.8(2)	2.18
$ \begin{array}{c} \operatorname{RuP} \\ \operatorname{(post} E_{\operatorname{app}} \operatorname{hold)} \end{array} $		1	7.7	2.4	1.08
$RuP_3$	1.216	1	6.0 (6)	6.3 (6)	0.40
$RuP_3$ (post $E_{app}$ )		1	14.5	13.3	0.18
RuPbpz	>1.62 <sup>c</sup>	1	11.9 (10)	2.1 (2)	1.01
RuPbpz $(post E_{app} hold)^d$		1	19.8	6.2	0.48

 $^aE_{\rm app}$  = 1.5 V (vs Ag/AgCl) unless otherwise noted. The values in parentheses indicate the expected values based on the molecular structure. The absorbance at the MLCT maximum before and after  $E_{app}$  hold for the indicated period of time are also gathered. <sup>b</sup>In this case, nanoITO was loaded for 10 min with RuP5OMe, followed by the overnight loading of  $4,4'-((HO)_2(O)P)_2$ bpy (p-bpy). <sup>c</sup>The potential is estimated from CV data of FTO|RuPbpz. dHeld at 1.9 V (vs Ag/AgCl) for 6 h.

than all other sensitizers. The trends observed in Figure 5 and Tables 1 and 2 clearly indicate that, by lowering the sensitizer reduction potentials,  $k_d$  will slow,  $%\Gamma_{cdm}$  will decrease, and the sensitizer Ru(III) stability will increase. Whereas d<sup>6</sup> Ru(II) analogues are coordinatively stabilized by  $d_{\pi}$ - $p_{\pi}$  back-bonding, d<sup>5</sup> Ru(III) has weaker back-bonding and, consistent with the expected high-oxidation state sensitizer coordination chemistry, enhances ligand substitution relative to Ru(II). Additionally, the formation of FTOlRuL-CDPs is effectively shut down by using a strong donor ligand like 4,4'-(MeO)<sub>2</sub>-2,2'-bipyridine. Other loss process(es) (via eqs 2b and 2c) are also still important because the overall  $\Gamma_{ret}$  percentage is smaller than 100% (Table 1). Furthermore, something fundamental is occurring at a Ru(III/ II) potential around 1.10 V, where decomposition begins to occur more rapidly. At 1.10 V versus Ag/AgCl (1.33 V vs NHE), it could be that the sensitizers have sufficient overpotential, (~150 mV) driving force, to appreciably affect non-catalytic water oxidation by the ruthenium center, which is consistent with the formation of Class 2 FTO|RuL-CDPs.

Decomposition to FTOlp-bpy becomes a more important process than desorption as the FTO|RuL Ru(III/II) reduction potential approaches the 1.39 V chemical decomposition threshold, but only after the Ru(III/II) potential is past 1.10 V. Below the 1.10 V threshold, desorption, not decomposition to FTOlp-bpy, is the primary loss mechanism. With FTOl RuP4OMe, ~80% ((100% $\Gamma_{max}(RuP4OMe)$ ) -- $40\%\Gamma_{ret}(RuP4OMe))/49\%\Gamma_{max}(RuP))$  of the lost sensitizer was accounted for with the readsorption of RuP.

Moving the sensitizer to nanoITO essentially eliminates the loss due to desorption for compounds that do not significantly decompose (i.e., compounds with  $E_{1/2}$  < 1.1 V). For example, application of a 1.5 V (vs Ag/AgCl) applied potential to nanoITO|RuP4OMe for 12 h resulted in nearly identical CV surface coverages ( $\%\Gamma_{ret} > 95$ ), UV-vis absorbances, and XPS spectra and indicates that net-desorption is essentially nonexistent with the mesoporous structure (Figure 7A). Whereas

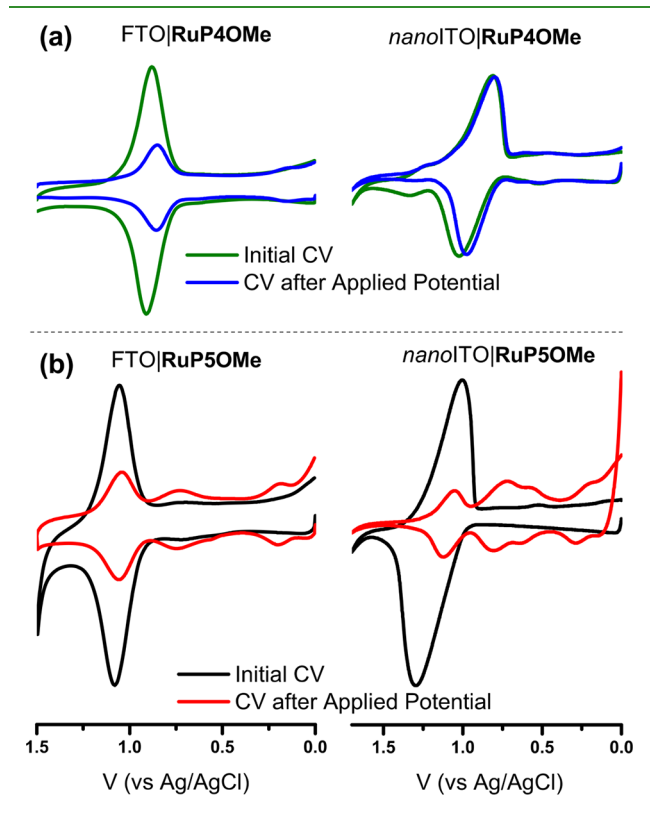


Figure 7. (A) CV overlay of FTO|RuP4OMe (left) and nanoITO| RuP4OMe (right) before applying a 1.5 V potential (green) and after applying a 1.5 V potential for 12 h (blue). (B) CV overlay of FTOI RuP5OMe (left) before (black) and after applying a 1.5 V potential for 4 min (red) and nanoITO|RuP5OMe (right) before applying a 1.5 V potential (black) and after applying a 1.5 V potential for 12 h (red). CVs on nanoITO were collected with a scan rate of 25 mV/s with a window from 0 to 1.7 V in aqueous 0.1 M HClO<sub>4</sub>. FTO|RuL scan rate = 100 mV/s from 0 to 1.5 V.

desorption from FTO|RuP4OMe results in loss of the desorbed sensitizer to the bulk solution, readsorption of diffusing RuP4OMe must be playing a significant role in enhancing the unprecedented stability of the sensitizer to harsh electrochemical oxidation.

However, only chemical decomposition according to eq 2a and eq 2c is taking place on nanoITO for complexes with  $E_{1/2}$ values larger than the 1.1 V threshold. For example, there is a significant difference in electrochemically active CDPs when comparing FTO|RuP5OMe to nanoITO|RuP5OMe (Figure 7B;  $\%\Gamma_{\rm cdm}$  = 22 (FTO; after 4 min applied potential) vs 60 (nanoITO; after 12 h of applied potential)). This observation is supported by XPS (Table 3). The phosphorus-to-nitrogen-toruthenium ratio remained almost unchanged after the 12 h applied potential experiment for nanoITO|RuP5OMe and nanoITO|RuP, alike.

The lower visible absorbance data are attributed to (1) less sensitizer resulting from chemical decomposition and (2) low molar absorptivities in the RuL-CDPs MLCT bands. Considering that RuL desorption to bulk solutions is shut down (as demonstrated with nanoITO|RuP4OMe and low absorption spectra of the bulk solutions following the 12 h experiment), the

enhanced production of nanoITO|RuP5OMe-CDPs may be the result of (1) readsorption of freely diffusing RuP5OMe followed by decomposition, (2) readsorption of RuP5OMe-**CDPs**, or (3) a combination of both.

Drastic increases in XPS phosphorus-to-nitrogen-to-ruthenium ratio indicates that compounds with very high Ru(III/II)  $E_{1/2}$  values rapidly undergo chemical decomposition at their non-adsorbed bpy ligands to generate electrochemically active CDPs (eq 2a) but eventually undergo adsorbed ligand substitution loss to nanoITO|p-bpy +  $\{Ru(L)_2^{2+}\}$  according to eq 3b. For example, in nanoITOlRuP3, the experimentally determined XPS Ru/N/P ratio, 1:6.0:1.8, is very close to the theoretical value of 1:6:2. After 12 h of oxidation, this ratio rises to 1:14.5:13.3, meaning that  $4,4'-((HO)_2(O)P)_2-2,2'-bipyr$ idine, or its decomposition products, 29 remains grafted on the surface, while the Ru center is lost to solution. Note that a similar process leading to the formation of TiO<sub>2</sub>I(HOOC)<sub>2</sub>-bpy has been observed, where the adsorbed carboxylated-bpy ligand remains adsorbed to the surface, while the Ru fragment decomposes into the solution.<sup>30</sup> The same analysis holds for nanoITO|RuPbpz.

Therefore, over the time scale of the experiment, complexes with redox potentials just above the 1.1 V threshold (i.e., RuP and RuP5OMe) maintain their kinetically controlled distribution of chemical decomposition products resulting from the substitution of non-adsorbed ligands, while complexes with higher redox potentials (i.e., RuP<sub>3</sub> and RuPbpz) are fluxional enough—due to the increased ligand labilization associated with higher potentials—to eventually undergo scission of the adsorbed phosphonated ligand from Ru.

Broader approaches to stabilizing sensitizers on oxide surfaces have been the subject of numerous studies. The incorporation of long-chain substituted ligands may not be desirable, because they significantly lower the driving force for photo-electrosynthetic processes. More versatile methodologies including poly(methyl methacrylate) (PMMA)<sup>31</sup> and fluoro-polymer overlayers,<sup>32</sup> electropolymerization,<sup>24,33</sup> and atomic layer deposition (ALD)<sup>34–38</sup> are at the forefront of many DSSC/ DSPEC studies and have been designed to eliminate entropic dissociation pathways. An alternative strategy that might prevent complete desorption would be the use of diazonium compounds, as recently reported.<sup>39</sup> These types of compounds were shown to be stable in a wide variety of conditions, and they lead to covalent bonds between the surface and the sensitizer. In the end, this should prevent full desorption of the sensitizer, but it is yet unclear the extent to which it would prevent chemical decomposition.

**Structural Effects.** Several structural parameters were taken into account to assess the overall stability of the sensitizer's monolayer. The substituents in the 5,5'-position of the 2,2'bipyridine ligands exhibited a greater effect than when the same substituents were introduced in the 4,4'-positions. This observation was striking for FTO|RuP5OMe and FTO| RuCP5OMe that were both lost ~100 times faster than their respective 4,4'-analogues FTO|RuP4OMe and FTO|RuC-P4OMe upon oxidation to Ru(III). Although very important, such an effect was expected, because the steric influence should be more pronounced at the 5,5'- or 6,6'-positions as compared to the 4,4'-positions. These data point to a bulkiness limit that a Ru(III) sensitizer can withstand at the 5,5'-positions and that the decomposition pathways are likely modified, once this limit is passed. Thus, repulsion between the FTO surface and bulky ligands, and possibly intraligand repulsion, increases the chemical decomposition rate constants,  $k_{2b}$  and  $k_{2c}$ , such that the electrochemically silent reactions (eq 2b and 2c) are favored over the pathway to FTO|RuP-CDPs (eq 2a). Nonetheless, the ~100 times increase in decomposition rate for the 5,5-OMe derivatives was almost negligible when the 5,5'-Me derivatives were used and indicates that such an increase in decomposition rates for the 5,5-OMe derivatives might not solely be due to increasing bulk. Different decomposition pathways could also be envisioned due to the stronger Lewis basicity of these 5,5'-OMe oxygen atoms as compared to those in 4.4'-OMe. For instance, protonation-induced decomposition or methoxy-to-quinone chemical transformations could also participate in additional decomposition pathways. At this stage, all of the aforementioned pathways could contribute to the overall decomposition and will be the subject of future studies.

Important data were obtained from the overall rigidity of the ligand by comparing FTO|RuPphen and FTO|RuP. The decomposition of the 1,10-phenanthroline complex occurred three orders of magnitude faster than the 2,2'-bipyridine system. Given the similar redox potential, it is suggested that the observed effects are sterically driven. Presumably, the induced steric interaction between the {RuII(phen)<sub>2</sub>} fragment and the FTO surface or neighboring RuPphen sensitizers serves as the driving force for loss of (1)  $Ru^{II}(phen)_2(p-bpy)(X)^{n+}$  or (2)  $\{Ru^{II}(p^{m+1})_2(X)_2^{m+1}\}$ , neither of which are electrochemically detectible under these experimental conditions, but both of which require that FTOlp-bpy must remain on the electrode surface. 40 Alternatively, it could be that 2,2'-bipyridine exhibits more degrees of freedom and is therefore able to accommodate the oxidation changes to a greater extent than the 1,10phenanthroline analogue.

Hydrophobicity seemed to have only a limited influence on the overall stability of the sensitizer in its oxidized form. Indeed, retention of FTO|RuIIIPtBubpy was nearly identical as FTO| Ru<sup>III</sup>P4Me, but a more significant effect was nonetheless observed for FTOlRuP<sup>t</sup>Bubpy in its reduced form. Very recently, Mulyana et al. reported on [Ru(4,4'-nonyl-2,2'bipyridine)(P) that exhibited stability in alkaline pH, a phenomenon that is unusual for phosphonate anchoring groups that tend to hydrolyze from the surface at pHs greater than 7. Overall, the structural effects seem to indicate that steric bulk and rigidity of the ligand play more important roles on the stability of the sensitizer's oxidized form than does the hydrophobicity. Decreased solubility of the sensitizer in water might also help improve the overall stability of the adsorbed layer.

### CONCLUSION

A series of ruthenium(II) sensitizers has been probed by electrochemistry, UV-visible spectroscopy, and XPS to investigate key factors affecting the stability of oxidized sensitizers as a model for long-term DSSC and DSPEC behavior. In all cases, Ru(II) forms are more stable than their oxidized forms, but desorption is still often observed. Oxidation to Ru(III) greatly accelerates the sensitizer loss via oxidatively induced ligand substitution (i.e., chemical decomposition) and desorption processes. Chemical decomposition to electrochemically active CDPs (i.e., where substitution occurs at the nonadsorbed ligands) strongly correlates to the sensitizer's Ru(III/ II) redox potential. Chemical decomposition is effectively inconsequential when the sensitizer's Ru(III/II) redox potential is below 1.10 V and complete above 1.39 V versus Ag/AgCl. Complete adsorbed ligand substitution is electrochemically

indistinguishable from desorption, but a simple reloading method and XPS data collected on nanoITOlRuL samples indicates that all processes are occurring for complexes with reduction potentials between 1.10 and 1.39 V. Changing the steric environment of the 4,4′-positions is inconsequential, while introducing substituents in the 5,5'-position resulted in faster decomposition. Restricting the geometry of the ligands accelerates decomposition, possibly by forcing decomposition to occur at the adsorbed ligand-metal bond rather than nonadsorbed 1,10-phenanthroline groups.

While the chemical decomposition of Ru-based sensitizers can be effectively eliminated by moving toward electron-rich ligand sets, desorption still plays a limiting role, and methods to prevent this loss mechanism represent a key challenge for optimizing device longevity on FTO electrodes. A tradeoff between these two processes must be considered: is FTOI RuP<sup>t</sup>Bubpy better than FTOlRuP4OMe with slightly more decomposition but enhanced retention? Part of the tradeoff of minimizing chemical decomposition comes at the cost of lowering the driving force for the DSSC/DSPEC devices; the relationship between redox potential and  $k_d$  or  $\%\Gamma_{cdm}$  presented in this report implies a fundamental limit for the use of these Ru coordination complexes for DSPECs, where high potentials are necessary to drive water oxidation but will intrinsically contribute to faster sensitizer decomposition. Hence, the results obtained here point toward the necessity of synthesizing new sensitizers with increasing stability in their oxidized form. Importantly, readsorption processes in nanocrystalline environment serve to mitigate the limiting desorption effects of a planar electrode environment and, in the case of nanoITO|RuP4OMe, very nearly approach the three criteria we set forth for an ideal electrochemically stable sensitizer:  $\%\Gamma_{\rm ret} = 100$ , a  $\%\Gamma_{\rm cdm} = 0$ , and a  $k_{\rm d} = 0 \, \rm s^{-1}$ .

All-in-all, key design features that will optimize the operational lifetime for Ru-based sensitizers in DSSCs and DSPECs include: minimizing time spent in the oxidized form, incorporating electron-donating groups, maximizing hydrophobicity, and minimizing molecular bulk near the adsorbed

### EXPERIMENTAL SECTION

General Considerations. CD<sub>3</sub>OD and D<sub>2</sub>O were obtained from Cambridge Isotopes Laboratories Inc. Solvents were used as received from Fisher Scientific. The following ligands were prepared according to literature methods: 5,5'-dimethoxy-2,2'-bipyridine, 42 2,2'-bipyrazine, 43 4,4'-dibromo-2,2'-bipyridine, 44 4,4'-trifluoromethyl-2,2'-bipyridine, 45 2,2'-bipyridine-4,4'-diphosphonic acid, 46,47 and 2,2'-bipyridine-4,4'-dimethylenephosphonic acid. 48 The following complexes we prepared according to literature methods: poly-Ru(1,4-cyclooctadiene)Cl<sub>2</sub>, <sup>49</sup> [Ru(phen)<sub>2</sub>Cl<sub>2</sub>], <sup>50</sup> Ru(MeObpy)(bz)(Cl)]. Cl, <sup>51</sup> [Ru(bpz)<sub>2</sub>Cl<sub>2</sub>]<sup>52</sup> RuP, <sup>12</sup> RuP<sub>2</sub>, <sup>12</sup> RuP<sub>3</sub>, <sup>12</sup> RuCP, <sup>12</sup> RuCP<sub>2</sub>, <sup>12</sup> RuP4Me, <sup>46</sup> RuP5Me, <sup>33</sup> RuP4OMe, <sup>46</sup> RuP<sup>t</sup>Bubpy, <sup>53</sup> RuCP<sub>3</sub>, <sup>12</sup> RuP4Me, <sup>46</sup> RuP5Me, KuP4OMe, RuPBr, <sup>46</sup> and RuPCF<sub>3</sub>, <sup>54</sup> See Figure 3 for associated structures. All and used without further purification.

Electrode Preparation. FTO was purchased in sheets from MTI Corporation (Tech 15) and cut to individual electrodes of dimensions 1.0 cm wide × 3.0-4.0 cm tall. FTO electrodes were cleaned by sonicating twice in isopropanol (iPrOH) for 20 min, twice in deionized H<sub>2</sub>O for 20 min, and then air-dried. Mesoporous nanoITO was prepared according to previously published procedures. 55,56 Sensitizer solutions (0.10-0.25 mM) in aqueous 0.1 M HClO<sub>4</sub> acid were prepared by first dissolving the sensitizer in deionized water, followed by the addition of the appropriate amount of 70%  $HClO_4$  (99.999% metal basis). RuPtBubpy and RuP3 were only slightly soluble in acidic water and hence were loaded on FTO or nanoITO from methanol or acetonitrile solutions. Solutions of the complexes were stored in a drawer (i.e., a dark place) during loading and long-term storage to prevent light-induced ligand substitution.

FTO surfaces were loaded by submerging the cut electrodes into sensitizer solutions for overnight or several days. Any precipitated, nonchemisorbed, or loosely adsorbed species were removed to achieve full monolayer surface coverage according to the following procedure: (1) rinsing the electrodes with ~15 mL of methanol, (2) sonicating the electrodes for 3 min in a vial containing MeOH, (3) rinsing with an additional ~15 mL of MeOH, and (4) carefully air-drying with compressed air. In the case of FTOlRuPtBubpy, the samples were sonicated for 1 h in N,N-dimethylformamide, rinsed with 15 mL of MeOH, and carefully air-dried.

nanoITO electrodes were immersed in sensitizer solutions for at least 3 h and rinsed with copious amounts of MeOH and then carefully dried with compressed air. The electrodes were not sonicated due to degradation of the nanoITO thin films.

Electrochemistry. Electrochemical measurements were conducted with CH Instruments 760D potentiostats or a Pine Wavedriver 10 Potentiostat/Galvanostat System in a three-compartment glass cell separated by medium- or fine-porosity frits to prevent interference from Cl<sup>-</sup> leaching from the reference electrode. The reference electrode and platinum counter electrode were placed in each of the outermost compartments, while the electroactive face of the FTO electrode was positioned toward the counter electrode. An RE-5B Ag/AgCl reference electrode with flexible connector (BASi model MF-2052) or a CH Instruments, Inc. CHI111 Ag/AgCl reference electrode with porous Teflon tip was used as the reference in aqueous solutions. Unless otherwise noted, all potentials are versus Ag/AgCl (+0.215 V vs NHE). HClO<sub>4</sub> (0.1 M; aqueous) was used as the electrolytic solution unless otherwise noted.

**Electrochemical Stability Protocol.** For sensitizers that survived 12 h of oxidation: the electrochemical protocol previously developed to monitor the behavior of FTO|RuP as a function of time was utilized. Specifically, the modified electrodes were placed in the central compartment of the three-compartment cell, described above, followed by (1) A series of three CV scans (0.0 to 1.5 V; sweep rate: 100 mV/s) to equilibrate the electrode prior to recording the initial voltammogram. A single CV scan (0.0 to 1.5 V; sweep rate: 100 mV/s) was then collected as time 0 in time-dependent experiments. (2) An applied potential  $E_{\rm app}$  hold of 1.5 V versus Ag/AgCl was applied for 30 min. (3) A single CV scan from 0.0 to 1.5 V at a sweep rate of 100 mV/s was recorded. The 30 min  $E_{\rm app}$  holds followed by single-cycle CV sequence was repeated 23 additional times with the total time held at 1.5 V of 12 h. The cycling process was automated by using a macro program written into the CHI760D software. Overlays of CV traces are not adjusted for current density for ease of plotting.

An identical procedure was followed for rapidly decomposing/ desorbing sensitizers, but applied potential times and applied potentials were modified to suit the particular sensitizer. Usually, the electrodes were subjected to an applied potential for 1 min, four times, as these produced similar % $\Gamma_{ret}$  as RuL surviving the 12 h protocol. For these compounds, the first anodic scan of each displayed only the  $E_{1/2}$ corresponding to the sensitizer, while the return cathodic scan, and subsequent scans, produced FTO|RuL-CDPs. The applied potential of 1.65 V was used for FTO|RuPCF<sub>3</sub> ( $E_{1/2} = 1.44 \text{ V}$ ) to ensure rapid and complete oxidation in accordance with the Nernst equation.

**Surface Coverages (\Gamma).** Surface coverages ( $\Gamma$  in mol/cm<sup>2</sup>) were determined from CV measurements by using eq 6. In eq 6, n is the number of electrons transferred per redox site (moles e<sup>-</sup>), F is the Faraday constant (96 485 C/mol), A is the area of the electrode  $(cm^2)$ , and Q<sub>Ep,c</sub> is the integrated charge for the cathodic surface Ru(III/II) wave from CV measurements.

$$\Gamma = \frac{Q_{E_{p,c}}}{nFA} \tag{6}$$

**Loss Rate Constant.** The loss rate constant  $k_{\rm d}$  has been reported previously and is elaborated briefly in the Supporting Information.<sup>2</sup>

Nuclear Magnetic Resonance. Characteristic NMR spectra were obtained at room temperature on a Bruker Avance 500 MHz spectrometer. Solvent residual peaks were used as internal standards for  $^{1}$ H ( $\delta$  = 3.31 ppm for CD<sub>3</sub>OD and 4.79 for D<sub>2</sub>O) chemical shift referencing. NMR spectra were processed using MNOVA.

Mass Spectrometry. Samples were analyzed with a hybrid LTQ FT (ICR 7T) (ThermoFisher) mass spectrometer. Samples were introduced via a microelectrospray source at a flow rate of 3  $\mu$ L/min. Xcalibur (ThermoFisher) was used to analyze the data. Each mass spectrum was averaged over 200 time domains. Electrospray source conditions were set as spray voltage 4.7 kV, sheath gas (nitrogen) 3 arb, auxiliary gas (nitrogen) 0 arb, sweep gas (nitrogen) 0 arb, capillary temperature 275  $^{\circ}$ C, capillary voltage 35 V, and tube lens voltage 110 V. The mass range was set to  $150-2000 \, m/z$ . All measurements were recorded at a resolution setting of 100 000. Solutions were analyzed at 0.1 mg/mL or less based on responsiveness to the electrospray ionization (ESI) mechanism. Low-resolution mass spectrometry (linear ion trap) provided independent verification of molecular weight distributions.

UV-Vis Absorption Spectroscopy. UV-Vis absorption spectra were recorded on a Varian Cary 60 UV-vis spectrophotometer with 1 nm resolution. For thin film slides, the samples were positioned at a  $45^{\circ}$ angle in quartz cuvettes with the FTO, solvent, and nanoITO background-subtracted.

Protocol for nanoITO Electrolysis and XPS Samples. All nanoITO samples were dyed from 0.1 M HClO<sub>4</sub> (aq) solution, except for RuP3 from acetonitrile, for 12 h prior to testing. Samples were presoaked in fresh 0.1 M HClO<sub>4</sub> (aq) solution for at least 1 h before electrochemical evaluation. Control samples for XPS that did not undergo electrochemistry were rinsed with copious amounts of methanol, then carefully dried with compressed air.

Electrochemical measurements were conducted on a BAS 100B potentiostat in a three-electrode setup, with the nanoITO sample as the working electrode, a RE-5B Ag/AgCl reference electrode with flexible connector (BASi model number MF-2052), and a platinum mesh counter electrode. Cyclic voltammetry was utilized before and after bulk electrolysis with a scan rate of 0.025 V s<sup>-1</sup>. For bulk electrolysis, samples were held at 1.5 V versus Ag/AgCl for 12 h except for RuPCF<sub>3</sub> (1.7 V for 6 h) and RuPbpz (1.9 V for 6 h). After bulk electrolysis, nanoITO slides were rinsed with copious amounts of methanol, then dried carefully with compressed air. These samples were then evaluated using XPS. The UV-vis absorption spectra of the resulting solutions were recorded in a quartz cuvette with 1.0 cm path length.

X-ray Photoelectron Spectroscopy. XPS was performed using a Kratos Axis Ultra-DLD spectrometer (Kratos Analytical Ltd.) with a base pressure of 5  $\times$  10<sup>-9</sup> torr equipped with a monochromatic Al K $\alpha$ source and a charge neutralizer. Survey and high-resolution spectra were taken with pass energies of 80 and 20 eV, respectively. Binding energies (BE) were found using BE = 284.6 eV for C 1s as a reference.

Microwave Reaction System. Microwave reactions were performed in an Anton Parr Monowave 300 microwave reactor. Typical conditions operate to reach the desired temperature in 3 to 5 min and are held at this temperature for a specific amount of time. After reaction, the system is cooled using a nitrogen flow to reach a temperature of 55 °C.

Synthetic Details for New Sensitizers. Synthesis of [Ru(5,5'-MeObpy)<sub>2</sub>Cl<sub>2</sub>]. Poly-Ru(1,4-cyclooctadiene)Cl<sub>2</sub> (500 mg, 1.78 mmol) and 5,5'-dimethoxy-2,2'-bipyridine (808 mg, 3.74 mmol) are heated at reflux for 2 h in 5 mL of o-dichlorobenzene. After reaction, the mixture is brought to room temperature and poured in 200 mL of diethyl ether. The precipitate is collected by filtration, washed with diethyl ether, and dried under vacuum. [Ru(5,5'-MeObpy)<sub>2</sub>Cl<sub>2</sub>] was obtained in an 87% yield and was used without further purification.

Synthesis of [RuP5OMe]. [Ru(5,5'-MeObpy)<sub>2</sub>Cl<sub>2</sub>] (110 mg, 0.18 mmol) and 2,2'-bipyridine-4,4'-diphosphonic acid (64 mg, 0.20 mmol) were suspended in 20 mL of a 1:1 EtOH/H<sub>2</sub>O mixture. The reaction mixture was heated at 160  $^{\circ}$ C for 20 min in a sealed microwave reaction vessel. After reaction, the mixture was taken to dryness. The residue was dissolved in water and filtered, and the filtrate was loaded on a size exclusion chromatography (LH20) column. Elution was performed using water as the eluent. The major orange band was taken to dryness, and the residue was triturated with diethyl ether and filtered. The title compound was obtained as an orange powder (103 mg, 62%). <sup>1</sup>H NMR (500 MHz, CD<sub>3</sub>OD)  $\delta$  8.92 (d, J = 12.7 Hz, 2H), 8.48 (dd, J = 9.2, 4.9 Hz, 4H), 7.98 (dd, J = 5.7, 3.2 Hz, 2H), 7.73 (qd, J = 10.0, 4.3 Hz, 6H), 7.28 (d, J = 2.7 Hz, 2H), 7.23 (d, J = 2.7 Hz, 2H), 3.82 (s, 6H), 3.78 (s, 6H)6H). HRMS (ESI-MS) m/z:  $[M]^{2+}$  Calcd for  $C_{34}H_{34}N_6O_{10}P_2Ru$ 425.0428; Found 425.0431.

Synthesis of [RuCP50Me]. [Ru(5,5'-MeObpy)<sub>2</sub>Cl<sub>2</sub>] (100 mg, 0.17 mmol) and 2,2'-bipyridine-4,4'-dimethylenephosphonic acid (63 mg, 0.18 mmol) were suspended in 20 mL of a 1:1 EtOH/H<sub>2</sub>O mixture. The reaction mixture was heated at 160 °C for 20 min in a sealed microwave reaction vessel. After reaction, the mixture was taken to dryness. The residue was dissolved in water and filtered, and the filtrate was loaded on a size exclusion chromatography (LH20) column. Elution was performed using water as the eluent. The major orange band was taken to dryness, and the residue was triturated with diethyl ether and filtered. The title compound was obtained as an orange powder (90 mg, 56%). <sup>1</sup>H NMR (500 MHz, CD<sub>3</sub>OD)  $\delta$  8.65 (s, 2H), 8.47 (dd, J = 9.3, 2.5 Hz, 4H), 7.74 (d, J = 5.8 Hz, 2H), 7.70 (td, J = 8.9, 2.7 Hz, 4H), 7.44 (d, J = 6.0 Hz, 2H), 7.26 (dd, J = 2.7, 1.7 Hz, 4H), 3.81(s, 6H), 3.76 (s, 6H), 3.33 (d, I = 16.5 Hz, 4H).  $[M]^{2+}$  Calcd for  $C_{36}H_{38}N_6O_{10}P_2Ru$  439.0584; Found 439.0588.

Synthesis of [RuCP<sub>2</sub>4OMe]. [Ru(MeObpy)(bz)(OTf)]·OTf (217 mg, 0.313 mmol) and 2,2'-bipyridine-4,4'-dimethylenephosphonic acid (225 mg, 0.654 mmol) were suspended in 40 mL of a 1:1 EtOH/ H<sub>2</sub>O mixture. The reaction mixture was heated at 160 °C for 20 min in a sealed microwave reaction vessel. After reaction, the mixture was taken to dryness. The residue was dissolved in water and filtered, and the filtrate was loaded on a size exclusion chromatography (LH20) column. Elution was performed using water as the eluent. The major orange band was taken to dryness, and the residue was triturated with a minimum amount of acetonitrile, filtered, and washed with diethyl ether. The title compound was obtained as an orange powder (200 mg, 49%).  $^{1}$ H NMR (500 MHz,  $D_{2}$ O)  $\delta$  8.36 (brs, 4H), 7.84 (brs, 2H), 7.68 (brs, 4H), 7.58-7.46 (m, 2H), 7.19 (m, 4H), 6.85 (brs, 2H), 3.87 (s, 6H), 3.42-3.03 (m, 8H). HRMS (ESI-MS) m/z:  $[M]^{2+}$  Calcd for C<sub>36</sub>H<sub>40</sub>N<sub>6</sub>O<sub>14</sub>P<sub>4</sub>Ru 503.02982; Found 503.02837.

Synthesis of [Ru(phen)<sub>2</sub>(P-ester)]. [Ru(phen)<sub>2</sub>Cl<sub>2</sub>] (80 mg, 0.15 mmol) and 2,2'-bipyridine-4,4'-diphosphonic ester (70 mg, 0.1 mmol) were dissolved in 10 mL of EtOH. The reaction mixture was heated at 160 °C for 30 min in a sealed microwave reaction vessel. After reaction, the mixture was taken to dryness. The residue was dissolved in methanol and filtered, and the filtrate was loaded on a size exclusion chromatography (LH20) column. Elution was performed using methanol as the eluent. The major orange band was taken to dryness, and the residue was triturated with diethyl ether and filtered. The title compound was obtained as an orange powder (75 mg, 52%). <sup>1</sup>H NMR (500 MHz, CD<sub>3</sub>OD)  $\delta$  8.90 (d, J = 12.0 Hz, 2H), 8.77 (d, J = 8.2 Hz, 2H), 8.67 (d, I = 8.2 Hz, 2H), 8.39–8.27 (m, 6H), 7.99 (d, I = 5.2 Hz, 2H), 7.90 (dd, J = 8.3, 5.2 Hz, 2H), 7.80 (dd, J = 5.7, 3.0 Hz, 2H), 7.67 (dd, J = 8.3, 5.2 Hz, 2H), 7.57 (dd, J = 11.1, 5.6 Hz, 2H), 3.94 (p, J = 7.1)Hz, 4H (hydroysis of two ester groups)), 1.23 (t, J = 7.1 Hz, 6H (hydroysis of two ester groups)). HRMS (ESI-MS) m/z: [M]<sup>2+</sup> Calcd for C<sub>38</sub>H<sub>34</sub>N<sub>6</sub>O<sub>6</sub>P<sub>2</sub>Ru 417.0529; Found 417.0536.

Synthesis of [RuPphen]. [Ru(phen)<sub>2</sub>P-ester] (45 mg, 0.041 mmol) was suspended in 4 mL of anhydrous acetonitrile. Trimethylsilyl bromide (60  $\mu$ L, 0.45 mmol) was added in a dropwise fashion. The reaction mixture was then stirred at 70 °C for 12 h. After reaction, the mixture was brought to room temperature, and 1 mL of methanol was added. The solvent was then removed under reduced pressure and triturated with diethyl ether to yield the title compound as a red powder (37 mg, 96%). <sup>1</sup>H NMR (500 MHz, CD<sub>3</sub>OD)  $\delta$  8.94 (d, J = 13.4 Hz, 2H), 8.79 (d, J = 8.3 Hz, 2H), 8.68 (d, J = 8.2 Hz, 2H), 8.33 (q, J = 8.9, 7.0 Hz, 6H), 7.99 (t, J = 4.7 Hz, 4H), 7.91 (dd, J = 8.3, 5.2 Hz, 2H), 7.70 Hz(dd, J = 8.2, 5.2 Hz, 2H), 7.64 (dd, J = 12.2, 5.6 Hz, 2H). HRMS (ESI-MS) m/z: [M]<sup>2+</sup> Calcd for C<sub>34</sub>H<sub>26</sub>N<sub>6</sub>O<sub>6</sub>P<sub>2</sub>Ru 389.0216; Found

Synthesis of  $[Ru(bpz)_2(P-ester)]$ .  $[Ru(bpz)_2Cl_2]$  (50 mg, 0.1 mmol) and 2,2'-bipyridine-4,4'-diphosphonic ester (55 mg, 0.13 mmol) were placed in a microwave reaction vessel containing 5 mL of a 1:1 EtOH/ H<sub>2</sub>O mixture. The reaction mixture was heated at 160 °C for 1 h. After reaction, the mixture was brought to room temperature and filtered on a fine-porosity frit. The filtrate was evaporated under reduced pressure, and the residue was purified on a size exclusion chromatography (LH20) column using methanol as eluent. The main orange band was collected and evaporated, and the residue was quickly purified on an Al<sub>2</sub>O<sub>3</sub> column using CH<sub>3</sub>CN/H<sub>2</sub>O 9:1 as the eluent. Purification through Al<sub>2</sub>O<sub>3</sub> column resulted in hydrolysis of one ester group of each -PO<sub>3</sub>Et<sub>2</sub> moiety. The product was obtained as an orange powder (71 mg, 77%). <sup>1</sup>H NMR (500 MHz, CD<sub>3</sub>OD)  $\delta$  10.00 (d, J = 1.1 Hz, 4H), 8.91-8.86 (m, 2H), 8.69 (dd, J = 8.7, 3.2 Hz, 4H), 8.03 (dd, J = 3.2, 1.2 Hz, 2H), 7.94 (dd, J = 3.2, 1.2 Hz, 2H), 7.84 (dd, J = 5.7, 3.1 Hz, 2H), 7.72 (m, 2H), 3.96 (p, J = 7.2 Hz, 4H), 1.26 (t, J = 7.1 Hz, 6H). HRMS (ESI-MS) m/z: [M]<sup>2+</sup> Calcd for  $C_{30}H_{30}N_{10}O_6P_2Ru$  395.0434; Found

Synthesis of [RuPbpz].  $[Ru(bpz)_2(P-ester)]^{2+} \cdot 2Cl^-$  (45 mg, 0.049) mmol) was dissolved in 4 mL of anhydrous acetonitrile. Trimethylsilyl bromide (52  $\mu$ L, 0.39 mmol) was added in a dropwise fashion. The reaction mixture was then stirred at 70 °C for 12 h. After reaction, the mixture was brought to room temperature, and 1 mL of methanol was added. The solvent was then removed under reduced pressure and triturated with diethyl ether to yield the title compound as an orange powder (41 mg, 94%). <sup>1</sup>H NMR (500 MHz,  $D_2O$ )  $\delta$  9.83–9.75 (m, 4H), 8.82-8.76 (m, 2H), 8.58 (m, 4H), 7.98 (dd, J = 3.4, 1.2 Hz, 2H), 7.94 (dd, J = 3.4, 1.3 Hz, 2H), 7.79 (dd, J = 5.7, 3.1 Hz, 2H), 7.63 (m, 2H). HRMS (ESI-MS) m/z: [M]<sup>2+</sup> Calcd for  $C_{26}H_{22}N_{10}O_{6}P_{2}Ru$  367.01212; Found 367.01059. [M-H+Na]<sup>2+</sup> Calcd for  $C_{26}H_{21}N_{10}NaO_6P_2Ru$  378.0031; Found 378.0012. [M-2H+2Na]<sup>2+</sup> Calcd for C<sub>26</sub>H<sub>20</sub>N<sub>10</sub>Na<sub>2</sub>O<sub>6</sub>P<sub>2</sub>Ru 388.9941; Found 388.9925.

### ASSOCIATED CONTENT

# Supporting Information

The Supporting Information is available free of charge on the ACS Publications website at DOI: 10.1021/acsami.8b04587.

FTO|RuL-CDPs interconversion figure, Laviron data tables and plots, CV figures for all compounds on FTO, CV and UV-vis data for nanoITO samples,  $k_d$ determination description, scheme outlining rotational ligand substitution mechanism, comprehensive loss mechanisms scheme, NMR data, XPS data, HRMS data (PDF)

## AUTHOR INFORMATION

# **Corresponding Author**

\*E-mail: HarrisonDP@VMI.edu.

#### ORCID

McKenzie M. Raber: 0000-0002-5174-0071 Matthew D. Brady: 0000-0002-3917-1072 Ludovic Troian-Gautier: 0000-0002-7690-1361 John C. Dickenson: 0000-0002-7788-6810 Jacob T. Hyde: 0000-0002-7910-3269 Santiago J. Lopez: 0000-0001-8963-3127 Gerald J. Meyer: 0000-0002-4227-6393 Thomas J. Meyer: 0000-0002-7006-2608 Daniel P. Harrison: 0000-0003-1840-2561

## Notes

The authors declare no competing financial interest.

## ACKNOWLEDGMENTS

D.P.H. acknowledges funding from the Virginia Military Institute (VMI) supporting the investigation of applied potentials and ligand effects on species stability. VMI Equipment Trust Funds and VMI Grants in Aid of Research funds

supported materials and instrument acquisition. M.M.R, J.C.D., and J.T.H. acknowledge support from the VMI Summer Undergraduate Research Institute. S.I.L. was supported by private departmental funds. M.D.B, S.L.M., and L.T.-G. acknowledge support from the UNC EFRC: Center for Solar Fuels, an Energy Frontier Research Center funded by the U.S. Department of Energy, Office of Science, Office of Basic Energy Sciences under Award No. DE-SC0001011 for synthesis and characterization of the ruthenium sensitizers as well as spectroelectrochemical measurements. The authors thank the Univ. of North Carolina Dept. of Chemistry Mass Spectrometry Core Laboratory and Dr. B. Ehrmann for assistance with mass spectrometry analysis. XPS measurements were performed at the Chapel Hill Analytical and Nanofabrication Laboratory, CHANL, a member of the North Carolina Research Triangle Nanotechnology Network, RTNN, which is supported by the National Science Foundation, Grant No. ECCS-1542015, as part of the National Nanotechnology Coordinated Infrastructure.

## REFERENCES

- (1) Alibabaei, L.; Brennaman, M. K.; Meyer, T. J. Light-Driven Water Splitting in the Dye-Sensitized Photoelectrosynthesis Cell. In *Molecular Devices for Solar Energy Conversion and Storage*; Tian, H., Boschloo, G., Hagfeldt, A., Eds.; Springer: Singapore, 2018; pp 229–257.
- (2) Brennaman, M. K.; Dillon, R. J.; Alibabaei, L.; Gish, M. K.; Dares, C. J.; Ashford, D. L.; House, R. L.; Meyer, G. J.; Papanikolas, J. M.; Meyer, T. J. Finding the Way to Solar Fuels with Dye-Sensitized Photoelectrosynthesis Cells. *J. Am. Chem. Soc.* **2016**, *138*, 13085–13102.
- (3) O'Regan, B.; Grätzel, M. A Low-Cost, High-Efficiency Solar Cell Based on Dye-Sensitized Colloidal  ${\rm TiO_2}$  films. *Nature* **1991**, 353, 737–740.
- (4) Concepcion, J. J.; House, R. L.; Papanikolas, J. M.; Meyer, T. J. Chemical Approaches to Artificial Photosynthesis. *Proc. Natl. Acad. Sci. U. S. A.* **2012**, *109*, 15560–15564.
- (5) Hagfeldt, A.; Boschloo, G.; Sun, L.; Kloo, L.; Pettersson, H. Dye-Sensitized Solar Cells. *Chem. Rev.* **2010**, *110*, 6595–6663.
- (6) Galliano, S.; Bella, F.; Gerbaldi, C.; Falco, M.; Viscardi, G.; Grätzel, M.; Barolo, C. Photoanode/Electrolyte Interface Stability in Aqueous Dye-Sensitized Solar Cells. *Energy Technol.* **2017**, *5*, 300–311.
- (7) Takijiri, K.; Morita, K.; Nakazono, T.; Sakai, K.; Ozawa, H. Highly Stable Chemisorption of Dyes with Pyridyl Anchors Over TiO<sub>2</sub>: Application in Dye-Sensitized Photoelectrochemical Water Reduction in Aqueous Media. *Chem. Commun.* **2017**, *53*, 3042–3045.
- (8) Yadav, S. K.; Ravishankar, S.; Pescetelli, S.; Agresti, A.; Fabregat-Santiago, F.; Di Carlo, A. Stability of Dye-Sensitized Solar Cells Under Extended Thermal Stress. *Phys. Chem. Chem. Phys.* **2017**, *19*, 22546—22554.
- (9) Mastroianni, S.; Lanuti, A.; Brown, T. M.; Argazzi, R.; Caramori, S.; Reale, A.; Di Carlo, A. Reverse Bias Degradation in Dye Solar Cells. *Appl. Phys. Lett.* **2012**, *101*, 123302.
- (10) Ji, Z.; He, M.; Huang, Z.; Ozkan, U.; Wu, Y. Photostable p-Type Dye-Sensitized Photoelectrochemical Cells for Water Reduction. *J. Am. Chem. Soc.* **2013**, *135*, 11696–11699.
- (11) Queyriaux, N.; Wahyuono, R. A.; Fize, J.; Gablin, C.; Wächtler, M.; Martinez, E.; Léonard, D.; Dietzek, B.; Artero, V.; Chavarot-Kerlidou, M. Aqueous Photocurrent Measurements Correlated to Ultrafast Electron Transfer Dynamics at Ruthenium Tris Diimine Sensitized NiO Photocathodes. *J. Phys. Chem. C* **2017**, *121*, 5891–5904.
- (12) Norris, M. R.; Concepcion, J. J.; Glasson, C. R. K.; Fang, Z.; Lapides, A. M.; Ashford, D. L.; Templeton, J. L.; Meyer, T. J. Synthesis of Phosphonic Acid Derivatized Bipyridine Ligands and Their Ruthenium Complexes. *Inorg. Chem.* 2013, 52, 12492–12501.

- (13) DiMarco, B. N.; Troian-Gautier, L.; Sampaio, R. N.; Meyer, G. J. Dye-Sensitized Electron Transfer from TiO<sub>2</sub> to Oxidized Triphenylamines that Follows First-Order Kinetics. *Chem. Sci.* **2018**, *9*, 940–949.
- (14) Hu, K.; Sampaio, R. N.; Marquard, S. L.; Brennaman, M. K.; Tamaki, Y.; Meyer, T. J.; Meyer, G. J. A High Valent Metal Oxo Species Produced by Photoinduced One Electron, Two Proton Transfer Reactivity. *Inorg. Chem.* **2018**, *57*, 486–494.
- (15) Dongare, P.; Myron, B. D. B.; Wang, L.; Thompson, D. W.; Meyer, T. J.  $[Ru(bpy)_3]^{2+*}$  Revisited. Is it Localized or Delocalized? How Does it Decay? *Coord. Chem. Rev.* **2017**, 345, 86–107.
- (16) Troian-Gautier, L.; Moucheron, C. Ruthenium<sup>II</sup> Complexes Bearing Fused Polycyclic Ligands: From Fundamental Aspects to Potential Applications. *Molecules* **2014**, *19*, 5028–5087.
- (17) Juris, A.; Balzani, V.; Barigelletti, F.; Campagna, S.; Belser, P.; von Zelewsky, A. Ru(II) Polypyridine Complexes: Photophysics, Photochemistry, Eletrochemistry, and Chemiluminescence. *Coord. Chem. Rev.* **1988**, *84*, 85–277.
- (18) Kalyanasundaram, K. Photophysics, Photochemistry and Solar Energy Conversion with Tris(bipyridyl)ruthenium(II) and its Analogues. *Coord. Chem. Rev.* **1982**, *46*, 159–244.
- (19) Zigler, D. F.; Morseth, Z. A.; Wang, L.; Ashford, D. L.; Brennaman, M. K.; Grumstrup, E. M.; Brigham, E. C.; Gish, M. K.; Dillon, R. J.; Alibabaei, L.; Meyer, G. J.; Meyer, T. J.; Papanikolas, J. M. Disentangling the Physical Processes Responsible for the Kinetic Complexity in Interfacial Electron Transfer of Excited Ru(II) Polypyridyl Dyes on TiO<sub>2</sub>. J. Am. Chem. Soc. **2016**, 138, 4426–4438.
- (20) Meyer, G. J. Molecular Approaches to Solar Energy Conversion with Coordination Compounds Anchored to Semiconductor Surfaces. *Inorg. Chem.* **2005**, *44*, 6852–6864.
- (21) Ardo, S.; Meyer, G. J. Photodriven Heterogeneous Charge Transfer with Transition-Metal Compounds Anchored to TiO<sub>2</sub> Semiconductor Surfaces. *Chem. Soc. Rev.* **2009**, *38*, 115–164.
- (22) Ashford, D. L.; Gish, M. K.; Vannucci, A. K.; Brennaman, M. K.; Templeton, J. L.; Papanikolas, J. M.; Meyer, T. J. Molecular Chromophore—Catalyst Assemblies for Solar Fuel Applications. *Chem. Rev.* **2015**, *115*, 13006—13049.
- (23) Hyde, J. T.; Hanson, K.; Vannucci, A. K.; Lapides, A. M.; Alibabaei, L.; Norris, M. R.; Meyer, T. J.; Harrison, D. P. Electrochemical Instability of Phosphonate-Derivatized, Ruthenium-(III) Polypyridyl Complexes on Metal Oxide Surfaces. ACS Appl. Mater. Interfaces 2015, 7, 9554–9562.
- (24) Ashford, D. L.; Lapides, A. M.; Vannucci, A. K.; Hanson, K.; Torelli, D. A.; Harrison, D. P.; Templeton, J. L.; Meyer, T. J. Water Oxidation by an Electropolymerized Catalyst on Derivatized Mesoporous Metal Oxide Electrodes. J. Am. Chem. Soc. 2014, 136, 6578–6581.
- (25) Eckermann, A. L.; Feld, D. J.; Shaw, J. A.; Meade, T. J. Electrochemistry of Redox-Active Self-Assembled Monolayers. *Coord. Chem. Rev.* **2010**, 254, 1769–1802.
- (26) Laviron, E. General Expression of the Linear Potential Sweep Voltammogram in the Case of Diffusionless Electrochemical Systems. *J. Electroanal. Chem. Interfacial Electrochem.* **1979**, *101*, 19–28.
- (27) These are not indicated in mechanistic equations for simplicity.
- (28) FTO|RuCP1→3 are not discussed, because methylene electrochemical oxidation complicated analysis.
- (29) Odrobina, J.; Scholz, J.; Risch, M.; Dechert, S.; Jooss, C.; Meyer, F. Chasing the Achilles' Heel in Hybrid Systems of Diruthenium Water Oxidation Catalysts Anchored on Indium Tin Oxide: The Stability of the Anchor. *ACS Catal.* **2017**, *7*, 6235–6244.
- (30) Karakus, M.; Zhang, W.; Räder, H. J.; Bonn, M.; Cánovas, E. Electron Transfer from Bi-Isonicotinic Acid Emerges upon Photodegradation of N3-Sensitized  ${\rm TiO_2}$  Electrodes. ACS Appl. Mater. Interfaces 2017, 9, 35376–35382.
- (31) Wee, K.-R.; Brennaman, M. K.; Alibabaei, L.; Farnum, B. H.; Sherman, B.; Lapides, A. M.; Meyer, T. J. Stabilization of Ruthenium-(II) Polypyridyl Chromophores on Nanoparticle Metal-Oxide Electrodes in Water by Hydrophobic PMMA Overlayers. *J. Am. Chem. Soc.* **2014**, *136*, 13514–13517.

- (32) Eberhart, M. S.; Wee, K.-R.; Marquard, S.; Skinner, K.; Wang, D.; Nayak, A.; Meyer, T. J. Fluoropolymer-Stabilized Chromophore—Catalyst Assemblies in Aqueous Buffer Solutions for Water-Oxidation Catalysis. *ChemSusChem* **2017**, *10*, 2380–2384.
- (33) Lapides, A. M.; Ashford, D. L.; Hanson, K.; Torelli, D. A.; Templeton, J. L.; Meyer, T. J. Stabilization of a Ruthenium(II) Polypyridyl Dye on Nanocrystalline TiO<sub>2</sub> by an Electropolymerized Overlayer. *J. Am. Chem. Soc.* **2013**, *135*, 15450–15458.
- (34) Lapides, A. M.; Sherman, B. D.; Brennaman, M. K.; Dares, C. J.; Skinner, K. R.; Templeton, J. L.; Meyer, T. J. Synthesis, Characterization, and Water Oxidation by a Molecular Chromophore-Catalyst Assembly Prepared by Atomic Layer Deposition. The "Mummy". Strategy. Chem. Sci. 2015, 6, 6398–6406.
- (35) Hanson, K.; Losego, M. D.; Kalanyan, B.; Ashford, D. L.; Parsons, G. N.; Meyer, T. J. Stabilization of  $[Ru(bpy)_2(4,4'-(PO_3H_2)bpy)]^{2+}$  on Mesoporous  $TiO_2$  with Atomic Layer Deposition of  $Al_2O_3$ . *Chem. Mater.* **2013**, 25, 3–5.
- (36) Hanson, K.; Losego, M. D.; Kalanyan, B.; Parsons, G. N.; Meyer, T. J. Stabilizing Small Molecules on Metal Oxide Surfaces Using Atomic Layer Deposition. *Nano Lett.* **2013**, *13*, 4802–4809.
- (37) Kim, D. H.; Losego, M. D.; Hanson, K.; Alibabaei, L.; Lee, K.; Meyer, T. J.; Parsons, G. N. Stabilizing Chromophore Binding on TiO<sub>2</sub> for Long-Term Stability of Dye-Sensitized Solar Cells Using Multicomponent Atomic Layer Deposition. *Phys. Chem. Chem. Phys.* **2014**, *16*, 8615–8622.
- (38) Song, W.; Vannucci, A. K.; Farnum, B. H.; Lapides, A. M.; Brennaman, M. K.; Kalanyan, B.; Alibabaei, L.; Concepcion, J. J.; Losego, M. D.; Parsons, G. N.; Meyer, T. J. Visible Light Driven Benzyl Alcohol Dehydrogenation in a Dye-Sensitized Photoelectrosynthesis Cell. J. Am. Chem. Soc. 2014, 136, 9773—9779.
- (39) Bangle, R.; Sampaio, R. N.; Troian-Gautier, L.; Meyer, G. J. Surface Grafting of Ru(II) Diazonium-Based Sensitizers on Metal Oxides Enhances Alkaline Stability for Solar Energy Conversion. *ACS Appl. Mater. Interfaces* **2018**, *10*, 3121–3132.
- (40) See additional discussion accompanying Figure S18.
- (41) Purnama, I.; Kubo, Y.; Mulyana, J. Y. A Robust Ruthenium Complex with Nonyl-Substituted bpy Ligand for Dye-Sensitized Photoelectrochemical Cell Application. *Inorg. Chim. Acta* **2018**, 471, 467–474
- (42) Fukuda, Y.; Seto, S.; Furuta, H.; Ebisu, H.; Oomori, Y.; Terashima, S. Novel Seco Cyclopropa[c]pyrrolo[3,2-e]indole Bisalkylators Bearing a 3,3'-Arylenebisacryloyl Group as a Linker. *J. Med. Chem.* **2001**, *44*, 1396–1406.
- (43) Boully, L.; Turck, A.; Plé, N.; Darabantu, M. Aryl-Aryl Bonds Formation in Pyridine and Diazine Series. Diazines Part 41. *J. Heterocycl. Chem.* **2005**, *42*, 1423–1428.
- (44) Staats, H.; Eggers, F.; Haß, O.; Fahrenkrug, F.; Matthey, J.; Lüning, U.; Lützen, A. Towards Allosteric Receptors Synthesis of Resorcinarene-Functionalized 2,2′-Bipyridines and Their Metal Complexes. Eur. J. Org. Chem. 2009, 2009, 4777—4792.
- (45) O'Donnell, R. M.; Sampaio, R. N.; Li, G.; Johansson, P. G.; Ward, C. L.; Meyer, G. J. Photoacidic and Photobasic Behavior of Transition Metal Compounds with Carboxylic Acid Group(s). *J. Am. Chem. Soc.* **2016**, *138*, 3891–3903.
- (46) Ashford, D. L.; Brennaman, M. K.; Brown, R. J.; Keinan, S.; Concepcion, J. J.; Papanikolas, J. M.; Templeton, J. L.; Meyer, T. J. Varying the Electronic Structure of Surface-Bound Ruthenium(II) Polypyridyl Complexes. *Inorg. Chem.* **2015**, *54*, 460–469.
- (47) Penicaud, V.; Odobel, F.; Bujoli, B. Facile and Efficient Syntheses of 2,2'-Bipyridine-Based Bis(phosphonic) Acids. *Tetrahedron Lett.* **1998**, 39, 3689–3692.
- (48) Neuthe, K.; Bittner, F.; Stiemke, F.; Ziem, B.; Du, J.; Zellner, M.; Wark, M.; Schubert, T.; Haag, R. Phosphonic Acid Anchored Ruthenium Complexes for ZnO-Based Dye-Sensitized Solar Cells. *Dyes Pigm.* **2014**, *104*, 24–33.
- (49) Doi, T.; Nagamiya, H.; Kokubo, M.; Hirabayashi, K.; Takahashi, T. Synthesis of a Tetrabenzyl-Substituted 10-Membered Cyclic Diamide. *Tetrahedron* **2002**, *58*, 2957–2963.

- (50) Servaty, K.; Moucheron, C.; Kirsch-De Mesmaeker, A. Trinuclear Ruthenium Dendrons Based on Bridging PHEHAT and TPAC Ligands. *Dalton Trans.* **2011**, *40*, 11704–11711.
- (51) Aliende, C.; Pérez-Manrique, M.; Jalón, F. A.; Manzano, B. R.; Rodríguez, A. M.; Espino, G. Arene Ruthenium Complexes as Versatile Catalysts in Water in Both Transfer Hydrogenation of Ketones and Oxidation of Alcohols. Selective Deuterium Labeling of rac-1-Phenylethanol. *Organometallics* **2012**, *31*, 6106–6123.
- (52) Bronner, C.; Wenger, O. S. Long-Range Proton-Coupled Electron Transfer in Phenol-Ru(2,2'-bipyrazine)<sub>3</sub><sup>2+</sup> Dyads. *Phys. Chem. Chem. Phys.* **2014**, *16*, 3617–3622.
- (53) Troian-Gautier, L.; DiMarco, B. N.; Sampaio, R. N.; Marquard, S. L.; Meyer, G. J. Evidence that  $\Delta S^{\ddagger}$  Controls Interfacial Electron Transfer Dynamics from Anatase TiO<sub>2</sub> to Molecular Acceptors. *J. Am. Chem. Soc.* **2018**, *140*, 3019–3029.
- (54) Brady, M. D.; Sampaio, R. N.; Wang, D.; Meyer, T. J.; Meyer, G. J. Dye-Sensitized Hydrobromic Acid Splitting for Hydrogen Solar Fuel Production. *J. Am. Chem. Soc.* **2017**, *139*, 15612–15615.
- (55) Farnum, B. H.; Morseth, Z. A.; Lapides, A. M.; Rieth, A. J.; Hoertz, P. G.; Brennaman, M. K.; Papanikolas, J. M.; Meyer, T. J. Photoinduced Interfacial Electron Transfer within a Mesoporous Transparent Conducting Oxide Film. J. Am. Chem. Soc. 2014, 136, 2208–2211.
- (56) Hoertz, P. G.; Chen, Z.; Kent, C. A.; Meyer, T. J. Application of High Surface Area Tin-Doped Indium Oxide Nanoparticle Films as Transparent Conducting Electrodes. *Inorg. Chem.* **2010**, *49*, 8179–8181.